Personalized microbiotas (counter-)select for antibiotic resistant strains

Authors

Michael Knopp[1,#], Sarela Garcia-Santamarina[1,4], Lina Michel[1], Dimitrios Papagiannidis[1], Sophia David[2], Denise M. Selegato[1], Joshua L. C. Wong[3], Nicolai Karcher[1], Gad Frankel[3], Michael Zimmermann[1], Mikhail M. Savitski[1], Athanasios Typas[1,#]

Affiliations

[1]Molecular Systems Biology Unit, European Molecular Biology Laboratory, Heidelberg, Germany

[2]Centre for Genomic Pathogen Surveillance, Pandemic Sciences Institute, University of Oxford, Oxford, United Kingdom

[3]Department of Life Sciences, Imperial College London, London, United Kingdom

[4]current address: Deep Microbiome Metabolomics, Hans-Knöll-Institute, Jena, Germany

Contacts

michael.knopp@embl.de and athanasios.typas@embl.de

Keywords

Antibiotic resistance, microbiome, evolution, *K. pneumoniae*, porins, nutrient competition

Abstract

Antibiotic resistant pathogens are an increasing public health threat, as development of novel therapeutics is outpaced by resistance emergence and dissemination. Approaches to slow down or even revert antibiotic resistance are necessary to maintain efficacy of both existing and new antibiotics. Such approaches exploit the fitness cost of resistance elements, but have largely relied on assessing this cost in laboratory conditions that poorly reflect the native context in which pathogens reside. Here we present a method that allows to investigate the influence of personalized human gut microbiota compositions on the competitive fitness of antibiotic resistant pathogens. Using fecal matter-derived microbiomes we identify a specific community that selects for a carbapenem-resistant *Klebsiella pneumoniae* strain. This selective advantage is due to mutations arising in a LacI-type transcriptional regulator, GlyR. We show that upregulation of the downstream glycoporin GlyP is causing the effect. By deconvoluting the microbiome composition, we identify a focal *E. coli* strain as a central driver of the selection, which is further modulated by other microbiota members. We demonstrate that the selective advantage is due to carbohydrate competition, and in particular for glycerol-containing compounds. Importantly, *glyR* mutations are under strong positive but conditional selection in clinical *K. pneumoniae* isolates. This implies a reduced competitiveness in other environments, which we experimentally validate *in vitro*. Overall, this study offers a path to identify microbiome-specific interactions that modulate the competitiveness of antibiotic resistant pathogens.

Introduction

The spread of antibiotic-resistant pathogens, combined with the lack of development of novel antibiotics, is a major challenge to modern medicine. In addition to reduced capacities to treat life-threatening infections, the spread of resistance jeopardizes life-saving medical procedures that rely on prophylactic antibiotic treatment, such as chemotherapy or surgical procedures[1]. In 2019 alone approximately five million deaths were associated with antibiotic resistant pathogens[2]. As the spread of resistant pathogens increases, deaths linked to them are expected to increase significantly over the next two decades if no decisive action is taken[3]. Despite the immense health and economic burden imposed by antibiotic resistance, development of novel antibiotics has lagged behind in the decades following the 'golden era of antibiotics' between 1940 to 1960, when most major classes of antibiotics were discovered[4,5]. Many reasons have contributed to this, including both challenges in identifying newly acting compounds and the broken antibiotic market. The result is that hardly any novel antibiotic classes have been introduced in clinical use for decades[4], with some hope that the tide will change with a new antibiotic class entering the market recently[6] and more candidates being in the pipeline[7-9]. Instead, most approved compounds in the last decades have been derivatives of antibiotics already in clinical use and are therefore prone to existing resistance mechanisms[10]. In addition to new antibiotics, the improvement of existing therapies can also help in dealing with the antibiotic crisis. This can be facilitated by exploiting drug synergies[11,12], optimizing drug dosing and delivery[13] or developing inhibitors for resistance determinants[14].

A different path to deal with the antibiotic crisis is to understand how cells develop resistance to them, and find ways to prevent, delay or counter-select this process. For example, many resistance determinants have been shown to cause cross-resistance (or collateral sensitivity) where increase in resistance to antibiotic A leads to increase in resistance (or susceptibility) to antibiotic B[15-18]. Treatment regimens can therefore be tailored to avoid pharmaceuticals that share resistance patterns or to combine drug pairs that lead to collateral sensitivity[19]. Although our current knowledge of drug collateral sensitivity is limited, especially since it depends on the pathogen and resistance mechanism, recent developments have opened ways to systematically identify, quantify and understand such drug relationships[20].

In addition to collateral sensitivity to specific compounds, antibiotic resistance acquisition can come with a 'fitness cost' in different environmental conditions[21]. Knowledge of such conditions opens the door for strategies to counter-select the resistant strain and/or promote its displacement by a susceptible strain[22], which can be treated with the antibiotic. Such strategies are particularly relevant for opportunistic pathogens, as removal of resistance can happen at their benign state, allowing for treatment when/if the bacterium becomes pathogenic. Traditionally, such fitness costs of antibiotic-resistance have been measured under axenic lab conditions by quantifying exponential growth rates or maximum yield. While this approach provides several benefits (high reproducibility, easy automation and low costs) and has been successfully employed for mechanistic studies of the effects of resistance acquisition on cellular physiology[23], it does not capture the complexity of the natural environments where pathogenic bacteria reside and antibiotic intervention takes place. For example, many opportunistic human pathogens reside together with other microbes in our body, where they compete for nutrients and niches[24]. The most prominent such microbial community is the human gut microbiome, which serves both as a reservoir for opportunistic pathogens and antibiotic resistance determinants[25-27]. With its diversity, complexity and multitude of interactions (e.g. from nutritional competition to cross feeding[28,29]), it poses a versatile challenge for the competitiveness of an antibiotic resistant bacterium, and at the same time an opportunity to identify strains, molecules and/or niches that expose the Achilles heel of resistance elements. Yet methods to do this are currently lacking.

Here, we present a method to capture fitness costs of antibiotic resistance within complex gut microbiomes, and use it to characterize the impact of diverse microbiome compositions on the fitness of the human pathogen *Klebsiella pneumoniae* carrying resistance determinants that are pervasive amongst clinical isolates causing hard-to-treat infections worldwide. We identify a specific microbiota that selects for the antibiotic-resistant isolate to evolve mutations in a LacI-type transcriptional regulator, which gives the strain a competitive advantage over its susceptible parent in utilizing glycerol containing sugars. This mutational signature emerges recurrently in clinical isolates, suggesting that the observed selective pressures exist in nature. At the same time, such variants seem to be an evolutionary dead end in clinics, likely due to reduced competitiveness in other environments. Consistently we show that these microbiome dependent selections are accompanied by severe tradeoffs in

107 utilization of other carbohydrates, which can be used for their rapid counter-selection. Overall,
108 this study exemplifies how we can utilize fecal matter derived microbiomes to identify
109 (counter-)selective pressures for resistant pathogens, which are prevalent *in vivo*.
110
111

112 Results

113 **A high-throughput method to quantify resistance-associated fitness costs within gut**
114 **microbiomes**

115 Bacterial fitness is typically determined by growth curve assays in axenic conditions or by
116 competition assays where the change in ratio of two competing strains is determined over
117 several passages[30]. The pairwise competition assays are more sensitive and can detect
118 interaction-dependent selective effects that are missed in monocultures. We decided to adapt
119 the classical pairwise-competition assay so it could be performed within a complex microbial
120 community setting, and assess how diverse microbiomes impact the competition of the two
121 focal strains (Fig. 1a, b; Methods).
122

123 We chose *K. pneumoniae* as our model strain due its classification as a priority human
124 pathogen[2,31], which is frequently associated with antibiotic resistance in clinical settings[32]. *K.*
125 *pneumoniae* is also a common member of the human gut microbiome[33], well studied, easy to
126 cultivate and genetically manipulate. We used a previously characterized isogenic set of *K.*
127 *pneumonia*e strains, which were chromosomally tagged with GFP or RFP markers to allow for
128 sensitive quantification with flow cytometry, and carried antibiotic resistance determinants
129 with minimal fitness effects during axenic growth in nutrient rich conditions[34]. These
130 comprised chromosomal mutations resulting into a loss-of-function deletion and pore-size
131 restriction of the two major porins OmpK35 and OmpK36, respectively (hereafter termed *K.*
132 *pneumoniae ompK*^{mut}) (Fig. 1c), and two clinically prevalent antibiotic resistance plasmids
133 encoding the carbapenemases KPC-2 and OXA-48 (pKpQIL-KPC2 and pOXA-48a). We set out
134 to perform pairwise competition assays between different versions of the resistant *K.*
135 *pneumonia*e strain and its susceptible parent, each carrying a different fluorescent marker
136 (and the marker swap; see methods) in different complex microbiota communities.
137

138 To assess different microbial community compositions, we chose nine native microbiomes
139 derived from fecal samples of healthy human adults (Fig. 1d), and one model synthetic
140 community of 21 different bacterial species that are prevalent in the human gastrointestinal
141 tract[35] and can provide colonization resistance to pathogens[36] (Fig. 1e). All communities were
142 stabilized in mGAM broth under anaerobic conditions for 72 hours with daily passaging, before
143 the two *K. pneumoniae* competitors were spiked into the different microbiomes at a 1:1:20
144 ratio and the community mix was passaged anaerobically for 4 days at a 1:1000 dilution every
145 24 hours, allowing for 10 doublings per day on average. After each passage, ratios of the
146 competitors (GFP or RFP positive), and the overall microbiome (untagged) counts, were
147 determined using flow cytometry. Thereby we could calculate the selection coefficients of the
148 competitors, i.e. the fitness effect per cell per generation, as well as the carrying capacity of
149 the different microbiomes for *K. pneumoniae*. Adapting the experimental setup to a 96 well
150 format, and using liquid-handling robots and a plate-based spectral analyzer, allowed us to
151 scale up the number of mutants/microbiomes tested, while maintaining high sensitivity (Fig.
152 1f). The initial total relative abundance of 10% *K. pneumoniae* when the competition coculture
153 was assembled decreased in all conditions by varying magnitudes. Most microbiomes showed
154 a steady decrease across every passage, suggesting that *K. pneumoniae* can not easily engraft
155 in some of these communities under the nutritional conditions present in mGAM. Abundance
156 stabilized at approximately 3-4% for the microbiomes, MB003 MB005 and MB007, and to <
157 1% for MB009 (Extended Data Fig. 1).
158
159 In the absence of a microbial community, *K. pneumoniae ompK*^{mut} was as fit as the wildtype,
160 whereas the pKpQIL-KPC2 and pOXA-48a plasmid acquisition led to a minor fitness cost of
161 roughly 1 and 2%, respectively (Fig. 1g). Most microbiomes did not cause a significant change
162 in the competitiveness of the antibiotic-resistant mutants or led to a slight reduction in the
163 fitness of *K. pneumoniae ompK*^{mut} and of its derivatives carrying the resistance plasmids –
164 strongest effect being 1.3-2% for MB001. In contrast to all other microbiomes, competing in
165 presence of MB003 let to *K. pneumoniae ompK*^{mut} outcompeting its parental susceptible
166 wildtype by about 4% per cell per generation – at least during later passages (Extended Data
167 Fig. 2). The effect was ameliorated by the presence of pKpQIL-KPC2 and pOXA-48a, as those
168 plasmids conferred fitness costs already in the absence of community. In contrast to all other
169 communities, the plasmid carrying variants were not outcompeted by the wildtype in

170 presence of MB003 (Fig. 1g). Altogether these results pointed to antibiotic resistance
171 determinants having microbiome-dependent fitness costs, and highlighted a specific effect of
172 MB003 that led to selection of the antibiotic resistance *K. pneumoniae* porin mutant.
173
174 **Microbiome MB003 drives the evolution of a high-fitness variant of the *K. pneumoniae***
175 **porin mutant**
176 The ratio changes in the competition experiments were constant over time across most
177 conditions, indicating stable fitness differences of the competitors throughout the experiment
178 (Extended Data Fig. 2), and allowing us to calculate selection coefficients (Fig. 1g). However,
179 replicates of the three pairwise competitions (*K. pneumoniae ompK*^{mut}, *K. pneumoniae*
180 *ompK*^{mut} /pOXA48 and *K. pneumoniae ompK*^{mut} /pKPC-2 versus *K. pneumoniae* wild type)
181 showed a large variation in MB003 (Fig. 1g). In fact, *K. pneumoniae ompK*^{mut} was initially
182 outcompeted by the susceptible wildtype in presence of MB003, and only increased in ratio
183 over the wildtype at later passages (Fig. 1h). This trajectory change during competition
184 experiments is indicative of a secondary mutation being selected during the experiment time
185 course that provides a fitness advantage to one of the competitors. To validate that an
186 underlying genetic change was driving the competitive advantage of the porin mutant in
187 MB003, we isolated the *K. pneumoniae ompK*^{mut} clones from the last day of the competition
188 experiment (hereafter termed *K. pneumoniae ompK*^{evo}), and competed them against the
189 wildtype. In line with our hypothesis, we observed a strong and consistent selective advantage
190 of *K. pneumoniae ompK*^{evo} (Fig. 1i) resulting in a fitness advantage of 7-8% per cell per
191 generation over the wildtype (Fig. 1j). The fitness advantage was specific for MB003, as the
192 evolved clones did not outcompete the wildtype in presence or absence of any of the other
193 microbiomes – with the exception of MB008 which resulted in a moderate fitness advantage
194 of 2% per cell per generation over the wildtype (Extended Data Fig. 3). Altogether we show
195 that MB003 provides a distinct selective milieu that drives the evolution of a *K. pneumoniae*
196 *ompK*^{mut} high-fitness variant able to outcompete the parental susceptible wildtype.
197
198 **A resident *E. coli* strain is driving the selection of a *K. pneumoniae* high-fitness resistant**
199 **mutant in microbiome MB003**
200 To determine the causative MB003 community member(s) for the enrichment of *K.*
201 *pneumoniae ompK*^{evo} we performed a metagenomic analysis of all nine fecal-derived

202 microbiomes (Fig. 2a). All microbiomes exhibited similar Shannon diversities, and contained
203 between 200 and 450 molecular operational taxonomic units (mOTUs)[37], with microbiome
204 MB007 having the least and MB001 having the most mOTUs. Strikingly, MB003 which strongly
205 enriched for *K. pneumoniae ompK*^{evo}, showed the most distinct metagenomic profile with a
206 dominance of Prevotellaceae. To identify which member(s) of microbiome MB003 contributed
207 to the selection of the high-fitness *K. pneumoniae ompK*^{evo} mutant, we chemically perturbed
208 MB003 in order to generate 48 subcommunities with reduced microbial complexity and
209 differential species abundances, as measured by 16S rRNA sequencing (see methods). All
210 subcommunities were then diluted in mGAM and inoculated with the *K. pneumoniae*
211 competitor pair, consisting of *ompK*^{wt} and the high-fitness variant *ompK*^{evo}. To exclude, that
212 the different conditions used to enrich the subcommunities affect the fitness of the different
213 *K. pneumoniae* strains, we performed the competition in pure mGAM. In contrast to previous
214 competition experiments we performed the co-culture competition experiment only for one
215 day as prolonged passaging in mGAM (without the subcommunity selective condition) would
216 likely shift the subcommunity composition causing inconsistent selective conditions. While
217 this experimental setup is less sensitive than the previous competition experiments and does
218 not allow us to calculate selection coefficients, we could qualitatively screen all
219 subcommunities for their selective effect on the evolved porin mutant by determining a
220 change in ratio from the 1:1 starting mixture to that after 24h of growth in presence of
221 different subcommunities (Fig. 2b). Most subcommunities enriched *K. pneumoniae ompK*^{evo}
222 over the wildtype in 24h of growth, but several subcommunities did no longer exhibit this
223 selective effect. The abundance of several genera showed a positive correlation with selection
224 of *K. pneumoniae ompK*^{evo} over the wildtype, such as *Sutterella, Parabacteroides* and
225 *Escherichia* (Extended Data Fig. 4, 5). The latter was of particular interest, as certain
226 conditions, such as bile salts, resulted in sub-communities dominated by *E. coli,* while
227 maintaining their selective effect on *K. pneumoniae ompK*^{evo} (Fig. 2b). To test whether *E. coli*
228 is sufficient to drive the selection of *K. pneumoniae ompK*^{evo}, we isolated the resident *E. coli* s
229 from MB003 (hereafter called *E. coli*^{MB003}) and showed that co-culturing it with the *K.*
230 *pneumoniae* competitors was enough for the *K. pneumoniae ompK*^{evo} to outcompete its
231 susceptible wildtype b 2% (Extended Data Fig. 6). Although subcommunities depleted for *E.*
232 *coli* (such as after sparfloxacin or cefotetan treatment) were still selective for *K. pneumoniae*
233 *ompK*^{evo} (Fig. 2b), we show that *E. coli* is sufficient to drive part of this selection.

234

235 **High-order epistatic interactions in microbial communities can modulate the selective**
236 **advantage of *K. pneumoniae ompK^{evo}* provided by *E. coli***

237 *E. coli* is a common member of the human gut microbiome[38] and present in all fecal
238 microbiomes used in this study (Extended Data Fig. 7), which raises the question why the
239 selection of *K. pneumoniae ompK^{evo}* occured only in presence of MB003. To determine how
240 specific the observed effect is to the *E. coli* strain isolated from MB003, we performed triple
241 competitions, consisting of *K. pneumoniae ompK^{wt}*, *K. pneumoniae ompK^{evo}* and as third
242 competitor, *E. coli* strains from a diverse panel of 85 laboratory, environmental and pathogenic
243 isolates[39], as well as three *E. coli* strains isolated from MB001, MB002 and MB003 (Fig. 3a).
244 The *E. coli* strains resulted into a wide range of selective coefficients for the *K. pneumoniae*
245 *ompK^{evo}*, ranging from no to approximately 4% fitness benefit. Notably in most cases in which
246 there was low/no selection for *K. pneumoniae ompK^{evo}*, this was linked to a poor ability of *E.*
247 *coli* to engraft in the community (Fig. 3a). This suggests that the selective effect exerted by *E.*
248 *coli^{MB003}* is a more general trait of *E. coli* rather than being specific to this strain. Corroborating
249 this, other *E. coli* strains isolated from fecal microbiomes used in this study also exhibited
250 strong selection (> 3% per cell per generation), even if their resident microbiome did not select
251 for the evolved porin mutant (Fig. 1g, 3a).

252

253 Given that the selective effect is generally provided by many *E. coli* strains, and that MB003
254 does not enrich for *E. coli* compared to the other microbiomes (Extended Data Fig. 7), it
255 implies that other microbiota members, besides the residential *E. coli* strains, play a role in
256 the selective effect and significantly modulate its magnitude. To address such potential higher-
257 order interactions, we performed quadruple competition experiments including as a fourth
258 competitor one further bacterial species relevant to the human gut microbiota (Fig. 3b). In the
259 competition experiment, we inoculated *K. pneumoniae ompK^{evo}*, *K. pneumoniae* wildtype, *E.*
260 *coli^{MB003}* and the fourth competitor in equal proportions and followed their abundance over
261 three days of competition. We also labeled *E. coli^{MB003}* with a chromosomally encoded YFP
262 marker to be able to follow the abundance of all four strains in the competition. The presence
263 of a fourth competitor (untagged) modulated the selective advantage of *K. pneumoniae*
264 *ompK^{evo}* exerted by *E. coli* in different ways. For example, the presence of other enterobacteria
265 or *Prevotella copri* increased the selective advantage of *K. pneumoniae ompK^{evo}* in presence

266 of *E. coli*^{MB003} to 3 percent, while the presence of *Clostridium perfringens* strongly alleviated
267 the fitness advantage. Notably, these modulating effects align with compositional differences
268 observed in MB003, which exhibits a low abundance of *Clostridiales* and a higher abundance
269 of *Prevotella* compared to the other fecal microbiomes (Fig. 2a). Collectively, our results
270 demonstrate that while *E. coli* is sufficient to provide a selective advantage of *K. pneumoniae*
271 *ompK*^{evo} over its ancestral susceptible wildtype, higher order interactions in the community
272 shape the magnitude and even direction of the selection. This is likely the reason we see the
273 selective advantage only in MB003, and not in other microbiomes.
274
275 **Microbiome MB003 selects for *glyR* mutations that lead to upregulation of an alternative**
276 **porin**
277 To elucidate the underlying molecular mechanism that allowed for the evolved porin-mutant
278 to benefit in presence of MB003, we whole-genome sequenced seven *K. pneumoniae ompK*^{evo}
279 clones. All strains had acquired a mutation in a LacI-type transcription factor hereafter termed
280 'glycoporin regulator' (*glyR*). The mutational spectrum spanned frameshifts and substitutions
281 causing premature stop codons, internal deletions and single amino acid substitutions namely
282 T60P, I54S and C248W (Fig. 4a). *glyR* is located upstream of three genes encoding a putative
283 permease, hydrolase and porin. This is a common organization of a carbohydrate catabolic
284 operon where the transcription factor regulates expression of the structural genes, which
285 facilitate sugar uptake through the outer- and inner- membrane, followed by its hydrolysis in
286 the cytoplasm. In line with this hypothesis, whole cell proteomes of all seven isolated *K.*
287 *pneumoniae ompK*^{evo} mutants exhibited consistently strong and specific upregulation of all
288 three proteins encoded in the structural genes (Fig. 4b and Extended Data Fig. 8).
289
290 To determine which of the structural genes are causing the fitness advantage of the *glyR*
291 mutant background when grown in presence of MB003, we constructed several knockout
292 variants. Removing the whole operon, the predicted transcription factor binding sites or all
293 three structural genes resulted in a complete loss of the fitness advantage phenotype,
294 confirming that indeed the structural genes upregulated in the *glyR* mutant background are
295 causative. Furthermore, knockouts of each of the individual structural genes revealed that the
296 porin alone was sufficient for the fitness advantage (Fig. 4c). The porin (hereafter termed
297 glycoporin, GlyP) is predicted to belong to the raffinose porin family RafY (Extended Data Fig.

298 9), which contains a larger pore size compared to OmpK35/36 and is involved in the uptake of
299 a range of carbohydrates including oligosaccharides[40,41].
300
301 **Carbohydrate competition drives the selective advantage of the *glyR* mutants**
302 There are several potential mechanisms of how an increased expression of GlyP would provide
303 a fitness advantage in a community context. Since porins are involved in nutrient uptake, it is
304 conceivable that the fitness benefit is based on an increased nutritional competence.
305 However, porins also play a role in the uptake of toxins, export of metabolic waste products
306 or as receptors of phage and conjugative plasmids[42-44]. As such, an outer membrane with
307 different porin composition could render *K. pneumoniae ompK*^{evo} able to use a new niche or
308 to be more resistant to toxic products or negative interactions with other community
309 members. To define the underlying mode of action of the evolved mutants, we grew *E.*
310 *coli*^{MB003} until saturation (20h), sterile filtered its supernatant, and used the spent medium to
311 determine growth characteristics of each *K. pneumoniae* strain in monocultures. *K.*
312 *pneumoniae ompK*^{evo} grew significantly better than its parental strains and the wild type in
313 the spent medium (Fig. 5a), demonstrating that the selective effect mediated by *E. coli* is
314 contact independent. Supplementing the spent medium with a good carbon source (0.2%
315 glucose), resulted in higher growth yields of all three *K. pneumoniae* strains (Fig. 5b), indicating
316 that a) the lack of carbon sources is growth-limiting for *K. pneumoniae* in these conditions,
317 and b) the selection advantage of *ompK*^{evo} is only visible in poor nutrient conditions and hence
318 most likely works via increased nutritional competence, as growth inhibitory mechanisms like
319 toxin uptake or phage susceptibility would have manifested independently of the absence or
320 presence of glucose.
321
322 MGAM is a rich medium designed to support the growth of a wide range of gut-derived
323 bacteria, and hence it contains a plethora of potential carbon sources that could create a
324 metabolic niche that selects for *K. pneumoniae ompK*^{evo}. To narrow down the spectrum of
325 potential candidate compounds, we performed thermal proteome profiling (TPP)[45,46]. Due to
326 the fact that enzyme-substrate interactions lead to thermal stabilization, TPP has the potential
327 to identify catabolic pathways that are thermally stabilized in *K. pneumoniae ompK*^{evo}, but not
328 in the *K. pneumoniae* wildtype, in the presence of the *E. coli*^{MB003} spent medium. Indeed, by
329 treating whole cell lysates of *K. pneumoniae* wildtype and *K. pneumoniae ompK*^{evo} mutant

330 with *E. coli*^{MB003} spent medium, we identified several proteins that were thermally stabilized
331 only in the *K. pneumoniae ompK*^{evo} lysate (Fig. 5c). In addition to GlyP itself, which was higher
332 expressed in the *ompK*^{evo} cells (Fig. 4b), two of the most strongly stabilized proteins in spent-
333 medium treated *K. pneumoniae ompK*^{evo} were DhaT and GlpK, both of which are involved in
334 glycerol catabolism. DhaT is the 1,3-propanediol dehydrogenase, which converts 3-
335 hydroxypropionaldehylde (generated from glycerol by a dehydratase) to 1,3-propanediol, and
336 GlpK is the glycerol kinase. The strong stabilization of both enzymes suggested that a) glycerol,
337 or glycerol-derivatives, were present in the spent media and b) that glycerol catabolic enzymes
338 were active in *K. pneumoniae ompK*^{evo} but not in the wildtype.
339
340 To determine whether glycerol or glycerol derivatives were available in the spent medium, we
341 decided to measure the metabolites present in the *E. coli*^{MB003} spent medium before and after
342 growth of *K. pneumoniae ompK*^{evo}. We chose eight different *E. coli* strains that were selective
343 for *K. pneumoniae ompK*^{evo} as well as three *E. coli* strains that were not (Fig. 3a), and prepared
344 spent medium of each strain individually. By profiling the growth of *K. pneumoniae* wildtype,
345 *K. pneumoniae ompK*^{mut} and *K. pneumoniae ompK*^{evo} in these spent media, we could confirm
346 that the growth characteristics in the various spent media (Extended Data Fig. 10) were
347 consistent with the selective coefficients determined in the co-culture experiments (Fig. 3a).
348 *K. pneumoniae ompK*^{evo} showed a growth advantage in spent media prepared from 'selective'
349 *E. coli* strains, while growing equally well to the wildtype in spent medium prepared from 'non-
350 selective' *E. coli* strains (Extended Data Fig. 10). We then subjected all spent media before and
351 after growth of *K. pneumoniae ompK*^{evo} to untargeted metabolomics to determine which
352 compounds were produced or consumed by *K. pneumoniae* (Fig. 5d). While we did not detect
353 free glycerol in the samples, we identified several glycerol-containing compounds that were
354 (i) present in mGAM, (ii) not consumed by *E. coli*, and (iii) consumed after growth of *K.*
355 *pneumoniae ompK*^{evo} (Fig. 5e and Extended Data Fig. 11). As such, Glyceryl-5-
356 hydroxydecanoate was significantly reduced in abundance in all spent-media prepared from
357 'selective' *E. coli* isolates. While also found in spent media derived from non-selective *E. coli*,
358 it was either consumed to a low degree (iAI16 and NT12033) or present at a lower levels (iAI16
359 NT12072) compared to spent media derived from 'selective' *E. coli*. Judging from the robust
360 growth of all *K. pneumoniae* strains in the spent media of non-selective *E. coli* strains

361 (Extended Data Fig. 10), it is likely that other better carbon sources are available to them, akin
362 to when glucose is present in the spent medium of *E. coli*^{MB003} (Fig. 5b).
363
364 To unambiguously show that selection of *K. pneumoniae ompK*^{evo} is due to an advantage to
365 catabolize glycerol, we performed competition experiments of *K. pneumoniae* wild type vs
366 either *K. pneumoniae ompK*^{mut} or *K. pneumoniae ompK*^{evo} in minimal medium supplemented
367 with glycerol or glucose as the sole carbon sources. While *K. pneumoniae ompK*^{mut} grew
368 similarly to the wildtype in glycerol, the *K. pneumoniae ompK*^{evo} exhibited a significantly
369 increased fitness of around 4% per cell per generation compared to the wildtype. This fitness
370 advantage was specific to glycerol as the evolved mutant grew similarly as the wildtype with
371 glucose as the sole carbon source (Fig. 5f). To determine if the selective advantage of *glyR*
372 mutants is specific for growth on glycerol, we tested a series of additional carbon sources for
373 their impact on fitness of *K. pneumoniae ompK*^{mut} and *K. pneumoniae ompK*^{evo} compared to
374 the wildtype. In stark contrast to growth on glycerol, we observed that other carbon sources,
375 such as fructose, lactose or maltose were counterselecting the *K. pneumoniae ompK*^{evo} with
376 counterselection coefficients reaching up to 9% per cell per generation.
377
378 In summary our results show, that treatment of *glyR* mutant lysates with *E. coli* spent medium
379 causes thermal stabilization of glycerol catabolic enzymes (indicating their metabolic activity),
380 that mGAM contains glycerol-derivatives that are consumed by *K. pneumoniae*, but not by *E.*
381 *coli* and that the *glyR* mutant has a selective advantage when grown in presence of glycerol
382 as the sole carbon source. This suggests that specific microbiota composition(s) can create a
383 niche for consumption of glycerol derivatives. This drives the selection of mutations in *glyR*,
384 which lead to increase in GlyP expression in the *ompK35/36* mutant.
385
386 ***glyR* mutations are under strong positive selection in clinical *K. pneumoniae* populations**
387 We next exploited a large collection of publicly-available genomes of the globally-important
388 high-risk lineage, clonal complex (CC) 258, which includes ST258 and other closely-related STs.
389 Thereby we could assess the sequence variation and evolution within the *glyP* operon, and
390 determine if the selective pressures identified in our *in vitro* screen are clinically relevant. In
391 particular, we generated a mapping-based chromosomal alignment of 9214 high-quality
392 CC258 genomes and used an ancestral reconstruction approach that, for each chromosomal

393 base position, inferred the ancestral base state at all nodes across a recombination-free
394 phylogenetic tree. For each base position, we then analyzed the occurrence and frequency of
395 base (state) changes across the phylogenetic tree, with a focus on the *glyP* operon. While the
396 structural genes within the operon showed only a few base changes with no more than 3 SNPs
397 occurring at any individual base position, we identified a single mutational hotspot (C->A) at
398 position 4,366,094 (with respect to the HS11286 reference genome), corresponding to the
399 T60P substitution in GlyR (Fig. 6a). We estimate that this substitution occurred independently
400 35 times across the CC258 phylogeny. Interestingly, we identified the same substitution in our
401 *in vitro* screening (Fig. 4a), confirming that the *in vitro* selection driven by MB003 in mGAM is
402 recapitulating selective pressures acting on clinical *K. pneumoniae* populations. Notably, we
403 also identified a distinct subclade in which *glyR* is entirely absent due to a deletion spanning
404 the gene (Fig. 6b, clade B). Consistent with this pattern, our *in vitro* screen also identified
405 premature stop codons and frameshift mutations in *glyR* (Fig. 4a).
406
407 Despite the *glyR* T60P mutation emerging frequently across the CC258 population, its sporadic
408 occurrence on terminal or near-terminal branches of the phylogenetic tree, and subsequent
409 presence in only 41/9214 (0.4%) of CC258 genomes, suggests that this mutation cannot
410 expand clonally (Fig. 6b). This is in contrast to what is expected for mutations that are under
411 long-term positive selection, which would expand within larger clades of the tree. This
412 absence of clusters is indicative, that *glyR* mutations are likely under strong positive selection
413 in some conditions, but then become disadvantageous and are quickly counter-selected when
414 conditions change. This is in line with our findings, that *K. pneumoniae ompK*^{evo} is only selected
415 in certain microbiomes (Fig. 1g), and that *K. pneumoniae ompK*^{evo} has no benefit, or even
416 strong fitness defects, when growing on other carbon sources than glycerol (Fig. 5f). Together,
417 these findings show that GlyP upregulation bestows a conditional selective advantage for *glyR*
418 mutations in *K. pneumoniae* in the presence of glycerol-containing niches, but these
419 mutations are an evolutionary dead-end when the available niche changes.
420

421 ## Discussion

422 Here, we determined the impact of diverse human gut microbiotas on the fitness of a
423 prevalent antibiotic resistance mutation in the ESKAPE pathogen *K. pneumoniae*. We

424 discovered that a specific microbiota drove the evolution of a high-fitness variant in the *K.*
425 *pneumoniae* resistant strain. The fitness benefit was caused by mutations in the
426 transcriptional regulator *glyR*, which resulted in the upregulation of an alternative porin, GlyP.
427 By using proteomic, metabolomic and phenotypic analyses we identified nutrient competition
428 for glycerol-containing compounds as the driving factor of the selection.
429
430 The general exclusion of intruding, usually pathogenic, species by the residential microbiota
431 is termed colonization resistance, and is an important property of a healthy microbiome.
432 Various studies have shown the benefit of resident/probiotic bacterial species in preventing
433 the invasion of pathogenic isolates[47-50]. Carbohydrate competition has been shown to play a
434 key role in colonization resistance against various pathogens, including, *E. coli*[49], *K.*
435 *pneumoniae*[48,51] and *S. enterica* serovar Typhimurium[47], where direct competition for
436 consumption of specific carbon sources such as galactitol or beta-glycosides can restrict
437 growth of pathogenic bacteria. Here we show that nutrients, and specifically glycerol
438 catabolism, drives the evolution and enrichment of an antibiotic resistant *K. pneumoniae*
439 porin-mutant. Although we showed that *E. coli* was at least partially responsible for the
440 creation of this selective niche, higher-order interactions with other community members
441 augmented or removed the selection. For example *Clostridium perfringens*, which removed
442 the selective niche. Interestingly, *E. coli* is unable to utilize glycerol as the sole carbon source
443 under strictly anaerobic conditions, while *K. pneumoniae* and members of the *Clostridiales*
444 family can[52-54]. Thus, we propose a model where *E. coli* is exerting its selective effect for the
445 high-fitness K. *pneumoniae* porin-mutant not by direct carbohydrate competition, but rather
446 by creating a niche by removing other, more favorable carbon sources.
447
448 Furthermore, we show that the selection for the high-fitness *K. pneumoniae* porin mutant is
449 context-dependent, as the *glyR* mutations are detrimental in other conditions. Clinical *K.*
450 *pneumoniae* isolates seem to be subjected to similar selective pressures, as shown by the
451 recurrent emergence of the *glyR* T60P mutation among clinical isolates. At the same time, and
452 in line with the results we presented here, the selective pressures are highly conditional,
453 limiting the clonal expansion *of K. pneumoniae* carrying *glyR* mutations. It is conceivable that
454 these mutations occur in isolated patients with favorable microbiome composition and dietary
455 habits, but are not competitive when the environment changes (diet or microbiome)

restricting their expansion and transmission. Identifying and understanding selective pressures against (high-fitness) antibiotic-resistant pathogens could enable us to drive off antibiotic resistant strains by dietary modulation.

Strategies for decolonization of pathogens from microbiomes are currently being discussed and actively researched. However counter-selection of an opportunistic pathogen from a 'healthy' microbiome opens a niche that could be covered by other invading pathogens. In contrast, finding conditions that specifically counter-select antibiotic-resistant variants of native opportunistic pathogens of the human gut microbiome (e.g. in *K. pneumoniae* or *E. coli*) would avoid this opening of the niche for new invaders. Instead this would allow the antibiotic susceptible strains of the same species to replace their resistant counterparts, and make treatment easier would the opportunistic pathogen lead to infection. Our study lays out a roadmap for how to identify potential probiotic bacteria and/or dietary compounds restricting growth of antibiotic-resistant bacteria that could subsequently be used to drive out antibiotic resistant pathogens from healthy gut microbiomes, decreasing the risk of acquiring hard-to-treat infections in the future.

472 **Materials and Methods**

473 Isolation of fecal microbiome samples

474 Fresh fecal samples from nine healthy donors were collected and transferred directly into an
475 anaerobic chamber. Samples were mixed at a 1:1 ratio (w/v) with PBS containing 40% glycerol
476 and 0.5 g/L cysteine, homogenized, and aliquoted into cryovials for preservation. At the time
477 of sample collection, one aliquot was inoculated into 50 ml of mGAM medium, serially diluted,
478 and incubated anaerobically at 37 ºC for 24 h. Following incubation, 800 µl of the diluted
479 cultures was combined with 200 µl of 50% glycerol and preserved at −80 ºC. The collection of
480 human stool samples and all related experiments were approved by the EMBL Bioethics
481 Internal Advisory Committee. Informed consent was obtained from all donors (BIAC2015-
482 009). The synthetic community was assembled as previously described. In brief, monocultures
483 of each species were grown overnight in mGAM broth anaerobically at 37 ºC, adjusted to
484 OD_{600} = 0.01, mixed at equimolar ratios and cryopreserved in 15% glycerol. For community
485 experiments, the frozen community was reconstituted in fresh mGAM by a 1:100 dilution and
486 grown for 24 hours in mGAM broth anaerobically at 37 ºC.

487

488 DNA extraction

489 Genomic DNA was isolated in 96-well deep-well plates. Cells were washed in PBS, and pellets
490 were resuspended in cell suspension solution (281 µl) from the GNOMETM DNA isolation kit
491 (MP Biomedicals). Resuspended cells were enzymatically digested with lysozyme (25 µl;
492 400,000 U ml−1, Sigma) at 37 ºC for 1h. Lysis was further enhanced by three freeze-thaw
493 cycles in liquid nitrogen, followed by the addition of the kit's lysis solution (15.2 µl) and RNA
494 mix (20 µl). A final lysis step was conducted using glass beads (Glasperlen, Edmund Bühler)
495 with bead-beating (5 min x 2 at 30 Hz) in a Tissue Lyzer II (Qiagen). Lysates were then incubated
496 at 37 ºC with shaking for 30 min, followed by protease treatment (12.8 µl; GNOMETM kit) at
497 55 ºC for 2h. Cell debris was removed by centrifugation (3200 g, 5 min) and 200 µl of the
498 supernatant was mixed with 100 µl of TENP buffer (50 mM Tris-HCl pH 8, 20 mM EDTA, 100
499 mM NaCl, 1% polyvinylpolypyrrolidone). The mixture was incubated for 10 min at 4 ºC with
500 75 µl of salt out solution (GNOMETM kit), followed by 10 min centrifugation at 3200 g. 200 µl
501 of supernatant was transferred to a fresh plate, mixed with 500 µl of ice-cold ethanol and 70 µl
502 of 3 M NaOAc pH 5.2 were added, and kept at −30 ºC overnight to precipitate DNA. The next

503 day, DNA was pelleted (3200 g, 45 min, 4 ºC), washed with 70% ethanol, air-dried, and
504 rehydrated in molecular-grade water at 4 ºC.
505
506 16S sequencing
507 For sequencing, 16S rRNA gene libraries were prepared using a two-step PCR approach with
508 Phire Hot Start II DNA Polymerase (Thermo Fisher Scientific). The V4 region was first amplified,
509 and a second PCR was carried out with indexed primers containing Illumina adaptors. Libraries
510 were sequenced using paired-end chemistry (2 x 250 bp) on a MiSeq platform.
511
512 Metagenomic sequencing
513 Microbial DNA was extracted from collected stool samples using Qiagen AllPrep PowerFecal
514 Pro DNA/RNA Kit (Qiagen, Hilden, Germany) following the manufacturer's protocol.
515 Metagenomic sequencing libraries were prepared using the NEBNext Ultra II DNA Library Prep
516 kit (New England Biolabs, MA, USA) with a targeted insert size of 350-400bp and Dual Index
517 multiplex oligos. Libraries were prepared using a liquid automated system (Beckman Coulter
518 i7 Series) and sequenced on an Illumina HiSeq 4000 platform (Illumina, San Diego, CA, USA)
519 with 2x150bp paired-end reads.
520
521 Preprocessing of 16S data
522 Raw sequencing reads from WGS and 16S data were processed using bbduk (v38.91). For WGS
523 data, reads underwent several preprocessing steps to remove low-quality sequences: Low-
524 quality bases were trimmed from both ends (qtrim = rl, trimq = 3), followed by the removal of
525 entire reads falling below a quality threshold (maq = 25). Adapter sequences were then
526 removed (ktrim = r, k = 23, mink = 11, hdist = 1, tpe = true, tbo = true) and reads shorter than
527 75 base pairs were discarded. For 16S data, reads underwent low-quality base trimming (qtrim
528 = rl, trimq = 10), followed by targeted removal of 5' amplicon primers from R1 and any
529 potential reverse complement primers from R2 (ktrim = l, k = 9, mink = 1, hdist = 1, restrictleft
530 = 50, maq = 20). Similarly, 3' primers were removed from R2, along with any potential reverse
531 complement sequences from R1 (ktrim = r, k = 9, mink = 1, hdist = 1, restrictright = 50, maq =
532 20). Finally, reads shorter than 75 base pairs were discarded.
533
534 Taxonomic profiling

535 For profiling of 16S data, we used IDTAXA84 from the DECIPHER package (v3.0.0)[55] with
536 parameters strand = both and threshold = 40 and the GTDB r207 (modified) training set. WGS
537 data were profiled using mOTUs (v3.1)[56] with default settings.
538
539 Community competition experiments
540 All competition experiments were performed at 37 ºC in an anaerobic chamber (Coy
541 laboratory Products; 2% H2, 12% CO2, 86% N2) in modified Gifu anaerobic medium (mGAM)
542 broth (HyServe, produced by Nissui Pharmaceuticals). For competitions in complex
543 communities, aliquots of the cryopreserved fecal microbiomes were thawed under anaerobic
544 conditions and 50µl were diluted in 5ml MGAM and grown overnight. The subsequent day,
545 the cultures were diluted in fresh mGAM broth to a final OD_{600} of 0.01. Overnight cultures of
546 the fluorescently labeled *K. pneumoniae* competitors were mixed at equimolar ratios and
547 added to the OD_{600}-adjusted communities at a final OD600 of 0.001, leaving a 10-fold excess
548 of community members compared to *K. pneumoniae* competitors. Each day, the competition
549 cultures were diluted 1:1000 in fresh mGAM broth to a final volume of 1ml. Each competition
550 experiment was conducted in two configurations: one in which strain A was tagged with GFP
551 and strain B with RFP, and another in which the fluorescent markers were reversed. Each
552 configuration was tested with a minimum of five biological replicates. Additionally, we
553 competed two independently constructed sets of the *K. pneumoniae* wild type carrying either
554 GFP or RFP with 10 biological replicates under each condition (microbiome) to determine the
555 fitness effect imposed by marker expression.
556 Competition in defined communities (triple competitions in presence of *E. coli* or quadruple
557 competition in the presence of an additional fourth competitor) were performed in a similar
558 fashion. Each competitor was grown overnight in mGAM and mixed at equimolar ratios to a
559 starting OD_{600} of 0.01. Competition experiments with defined carbon sources were performed
560 in M9 minimal medium (0.1 mM $CaCl_2$, 1mM $MgSO_4$, 1x M9 Salts (Sigma Aldrich))
561 supplemented with the carbon source of interest at a final concentration of 0.2%.
562 To determine the ratios of GFP^+, RFP^+ or GFP^-/RFP^- cells, 50µl aliquots were removed from
563 each passage, washed twice with PBS and samples were resuspended in 50µl PBS. The
564 samples were incubated for 2h at room temperature under aerobiosis to allow maturation of
565 the fluorescent proteins. After two hours cells were fixed by adding an equal amount of 4%
566 Paraformaldehyde and incubating for 10 minutes. After fixation, cells were washed once with

567 PBS and taken up in 150µl final volume PBS. Samples were subjected to flow cytometry to
568 determine the ratio of the RFP^+ and GFP^+ competitors, as well as the untagged microbiome
569 using the Aurora spectral analyzer (Cytek Biosciences). In rare cases, individual wells were
570 excluded from analyses where fluorescent populations could not be clearly distinguished from
571 non-fluorescent background events, likely due to incomplete resuspension before aeration
572 causing a failure in fluorescent protein maturation.
573
574 Whole genome sequencing
575 To isolate the endpoint *K. penumoniae* strains, competition cultures were streaked out on LB
576 (5 g yeast extract, 10 g Tryptone, 10 g NaCl L^{-1}) Agar plates containing 50 mg/L Carbenicillin
577 and incubated aerobically at 37°C overnight, which specifically selects for the growth of K.
578 pneumoniae. GFP or RFP tagged colonies were differentiated using a Flu-O-Blu
579 transilluminator (Biozym). Colonies of interest were purified by streaking on LB agar plates
580 and incubating at 37 °C overnight. The isolates were then grown overnight in LB broth and
581 cryopreserved using 15% glycerol. 1 ml of each culture was used to extract genomic DNA
582 using the MasterPure DNA purification kit according to the manufacturer's recommendations
583 (Epicentre). All samples were subjected to whole-genome sequencing using a MiSeq system
584 (Illumina, USA). The paired-end sequence reads were trimmed and mapped using CLC
585 Genomics Workbench (CLC Bio, Denmark) using standard parameters. Subsequently,
586 inversion, deletions, structural variants, and single nucleotide polymorphisms were
587 determined using standard parameters.
588
589
590 Subcommunity enrichment
591 Forty-eight growth conditions were established (Supplementary Table X). Drug compounds,
592 except rifaximin which was freshly prepared, were dissolved as 100x stock solutions in
593 ethanol, DMSO, or water, as appropriate, and stored at −20 °C in 96-well drug plates. Rich and
594 selective media were freshly prepared and stored at room temperature. Twenty-four hours
595 prior to inoculation, all materials and reagents were transferred into an anaerobic chamber
596 (Coy Laboratories). On the day of inoculation, drug/medium plates were assembled under
597 anaerobic conditions by mixing 100 µl of medium with the compounds in the drug plate,
598 followed by transfer of 115 µl of the resulting drug–medium mixture back into the deep-well

599 plate. For medium-no drug conditions, 1,485 µl of medium was added to the corresponding
600 well.
601 Cryopreserved stool from donor MB003 (700 µl aliquot, prepared as described above) was
602 diluted 1:100 in PBS, and 15 µl of this suspension was inoculated into each of the 48 wells of
603 a 96-well deep-well plate containing 1,485 µl of medium (~5×10^7 CFU ml^{-1} final). Cultures
604 were incubated anaerobically at 37 °C for 24 h, then sequentially passaged for three additional
605 days by 1:50 dilution into fresh drug/medium plates. Growth was monitored daily by
606 transferring 100 µl of culture into shallow 96-well plates and measuring optical density at 578
607 nm every hour for 24 h. On day 5, 500 µl of each culture was mixed with glycerol for long-term
608 storage, and the remaining culture (~1 ml) was collected for DNA extraction.
609 E. coli was isolated from the bile-salt-treated subcommunity by plating on LB agar plates and
610 incubating at 37°C under aerobic conditions overnight. Colonies were purified and species was
611 determined by 16S sequencing. After confirmation, that the isolated *E. coli* strain is selective
612 for *K. pneumoniae ompK*^{evo}, whole genome sequencing of the strain was performed as
613 described previously.
614
615 Construction of knockout mutants
616 Gene knockouts were constructed using the lambda red recombineering system encoded on
617 the synthetic vector pSIM5-tet [57,58]. Overnight cultures of the strain of interest were diluted
618 1:100 fold in 50 ml LB broth at 37°C with constant shaking to a final OD600 of 0.2. Cells were
619 harvested and washed three times with ice gold 10% glycerol and taken up in a final volume
620 of 100µl. 40µl cells were mixed with 50 ng of pSIM5 tet and transferred to an electroporation
621 cuvette (1-mm gap). Electroporation was performed using a Gene Pulser (Bio-Rad) at 1.9kV,
622 400 Ohm and 25µF. After electroporation, cells were recovered in 1ml SOC (2% trypton, 0.5%
623 yeast extract, 10 mM NaCl, 2.5 mM KCl, 10 mM $MgCl_2$, 10 mM $MgSO_4$ and 20 mM Glucose)
624 for 2 hours, plated on LB Agar plates containing 10 mg/L tetracycline and incubated at 30°C.
625 Successful transformants were grown overnight in LB broth containing 10 mg/L tetracycline at
626 30°C.
627 To prepare electrocompetent cells, pSIM5-tet carrying strains were grown overnight in LB
628 broth supplemented with 10 mg/L tetracycline at 30°C, diluted 1:100 in 50 ml LB broth
629 supplemented with 10 mg/L tetracycline and incubated at 30° until they reached OD600 =
630 0.02. Cultures were moved to a 42°C waterbath to induce expression of the lambda red system

631 for 15 minutes. Afterwards, the cultures were placed on ice for 10 minutes and washed 3 times
632 with ice-cold 10% glycerol. The cells were taken up in 200µl 10% glycerol final volume, and
633 40µl were mixed with a 200 ng purified PCR product of a gene construct containing *amilCP*
634 (blue chromoprotein), *cat* (chloramphenicol resistance) and *sacB* (sucrose sensitivity) with
635 homologous overhangs up- and downstream of the gene of interest. Electroporation was
636 performed using a Gene Pulser (Bio-Rad) at 1.9kV, 400 Ohm and 25µF. After electroporation,
637 cells were recovered in 1 ml SOC (2% trypton, 0.5% yeast extract, 10 mM NaCl, 2.5 mM KCl,
638 10 mM $MgCl_2$, 10 mM $MgSO_4$ and 20 mM Glucose) for 2 h. Successful transformants were
639 selected on LB agar plates supplemented with 15 mg/L chloramphenicol at 30°C.
640 Transformants were restreaked on LB agar plates supplemented with 10 mg/L tetracycline at
641 30°C to ensure maintenance of pSIM5-tet. The strains were then subjected to a second round
642 of transformation as described above. Here, instead of a PCR product, single-stranded DNA
643 was electroporated composed only of the up- and down-stream homologuous overhangs, to
644 replace the amilCP-cat-sacB cassette leaving a scar-free knockout. Recovery of transformants
645 was performed in 5 ml SOC overnight to ensure complete removal of the SacB protein, and
646 successful transformants were selected on salt-free LB agar plates supplemented with 5%
647 sucrose. Loss AmilCP, and therewith loss of the blue colour, was an additional verification, that
648 the complete amilCP-cat-sacB cassette was removed, and sucrose sensitivity was not only lost
649 due to a loss-of-function mutation in *sacB*. All final constructs were confirmed by sanger
650 sequencing.
651
652
653 <u>Growth characterization in spent medium</u>
654 To prepare spent medium an overnight culture of the E. coli strain of interest was diluted
655 1:1000 in 20 ml mGAM under anaerobic conditions. The culture was grown for 20h, and cells
656 were pelleted by centrifugation for 10 minutes at 4000 rpm. The supernatant was transferred
657 and subjected to a second round of centrifugation for 10 min at 4000 rpm. The supernatant
658 was sterile filtered using a filter with a 0.22µm pore size. The filtered supernatant was then
659 brought back to anaerobic conditions and used as 'spent medium broth' for growth
660 characterization of the *K. pneumoniae* isolates. For this, overnight cultures of K. pneumoniae
661 in mGAM were diluted 1:2000 in spent medium. Growth rate was determined in 96-well plates
662 sealed with breathable membranes and OD600 was determined in 20-minute intervals over

663 24hours using a Filtermax F5 multimode plate reader (Molecular Devices). The first timepoint
664 was used for background subtraction. All growth rate determinations were performed in
665 triplicate.
666
667
668 Estimating the occurrence and frequence of SNPs across the *glyP* operon among *K.*
669 *pneumoniae* CC258 genomes
670 We generated a large collection of CC258 genomes from publicly-available genomes available
671 in Pathogenwatch (https://pathogen.watch)[59]. Raw sequence reads associated with these
672 genomes were downloaded from the European Nucleotide Archive (ENA) using available
673 accession numbers. Reads were mapped to the ST11 reference genome, HS11286 (accession
674 CP003200) using a workflow (https://gitlab.com/cgps/ghru/pipelines/snp_phylogeny)
675 (version 1.2.2) incorporating BWA-MEM (Li, 2013), SAMtools and BCFtools[60] and a pseudo-
676 genome alignment was generated. Genomes were excluded from downstream analyses if they
677 had <20x average mapping depth or ≥25% missing sites in the pseudo-genome alignment.
678 Gubbins v3.2.1[61] was used to remove recombined regions from the alignment and generate a
679 maximum likelihood tree with RAxML-NG[62]. For each base position within the pseudo-
680 genome alignment, a maximum parsimony method was used to perform ancestral
681 reconstruction across the tree (https://github.com/sanger-pathogens/bact-gen-
682 scripts/blob/master/reconstruct_snps_on_tree.py). The number of state changes inferred to
683 have occurred across the tree at each base position was calculated and the types of SNPs
684 recorded.
685
686
687 Genotypic characterisation of genome assemblies
688 Genome assemblies from the above-described CC258 collection were additionally
689 characterised. Kleborate v2.3.0 was used to identify virulence and resistance genes including
690 alterations within the *ompK35* and *ompK36* porin genes[63]. These included truncations of both
691 genes, and loop 3 insertions (glycine-aspartate (GD) or threonine-asparate (TD)) within
692 *ompK36*. The lacI type transcription factor gene was identified among the assemblies using
693 BLASTn v2.14.1[64] with the full-length gene from ATCC43816 (accession CP009208) as the
694 query sequence. We required a single hit of the gene in each assembly that matched ≥25% of

695 the query length and contained a start codon to unambiguously identify the gene. Nucleotide
696 sequences were translated to protein sequences using Seaview v5.0.5[65] with the standard
697 genetic code. Protein sequences were predicted to be intact if they possessed at least 90% of
698 the query length. Metadata and genotypic data were visualised with the phylogenetic trees
699 using Microreact v273[66].
700 The Artemis Comparison Tool (ACT) v18.1.0[67] was used to compare the ST11 genome,
701 HS11286, with a representative genome assembly from the clade of 306 CC258 isolates with
702 an absent lacI type TF gene (SRR12509433). Prior to the comparison, the contigs from
703 SRR12509433 were aligned and reordered against the HS11286 complete genome using
704 Abacas v1.3.1[68].
705
706
707 Metabolite extraction
708 LC-MS grade solvents were purchased from Fisher Scientific, and all other chemicals from
709 Sigma Aldrich, unless otherwise specified. For metabolite extraction, 20 µL of the bacterial
710 supernatants were transferred in a 96-well plate with 105 µL of ACN:MeOH solvent mixture
711 in a 1:1 ratio supplemented with an internal standard mixture. The internal standard mixture
712 contained sulfamethoxazole, caffeine, ipriflavone, and warfarin, each at 80 nM final
713 concentration. Following, the samples were chilled at -20°C for 1 h to allow proteins to
714 precipitate, then centrifuged at 4500 rpm for 15 min at 4 °C. The remaining supernatant was
715 finally aliquoted in 96-well microtiter plates, diluted with water (1:1), and an additional
716 centrifugation step at 4500 rpm for 15 mins and 4 °C.
717
718
719 LCMS analysis
720 LC-MS analysis was performed using reverse-phase chromatography in negative ionization
721 mode. Chromatographic separation was performed using an InfinityLab Poroshell 120 HILIC-Z
722 column (2.1 x 150 mm, 2.7-micron pore size) in an Agilent 1200 Infinity UHPLC system and
723 mobile phases A: H_2O + 5mM Ammonium formate + 0.1% formic acid and B: acetonitrile +
724 5mM Ammonium formate + 0.1% formic acid. The column compartment was kept at 25°C. 5
725 µL of the sample was injected at 98% B and 0.250 mL/min flow followed by: 98% B until minute
726 3, a gradient to 70% B until minute 11, a gradient to 60% B until minute 12, a gradient to 5%

727 B to minute 16, remaining at 5% until minute 18 before re-equilibration to 98% until minute
728 20. Flow remained at 0.250 mL/min.
729 The qTOF (Agilent 6550) was operated in positive scanning mode (50 – 1500 *m/z*) and
730 electrospray ionization (ESI) with the following source parameters: VCap: 3000 V, nozzle
731 voltage: 0 V, gas temp: 225 °C; drying gas 11 L/min; nebulizer: 40 psig; sheath gas temp 225°C;
732 sheath gas flow 10 L/min; fragmentor 300V and Octopole RF Vpp 450V. Online mass
733 calibration was performed using a second ionization source and a constant flow of reference
734 solution (121.0508 and 922.0097 *m/z*).
735 Tandem mass spectrometry analysis (LC-MS/MS) was performed for all significant
736 metabolites using the chromatographic separation and source parameters described above
737 and the targeted-MS/MS mode of the instrument with a preferred inclusion list for parent ion
738 with 20 ppm tolerance, Iso width set to 'narrow width', and collision energy set to either 10,
739 20, or 40 eV.
740
741 Data Extraction and Statistical Analysis
742 To reduce data complexity for downstream analysis, mass spectrometry data were
743 centroided and converted from the proprietary format (.d) to the m/z extensible markup
744 language format (.cef) using the peak picking algorithm of Agilent DAReprocessor at the
745 following parameters: minimum peaks height >= 5.000 counts; all ion species; only select
746 common organic compounds (no halogens); isotoping grouping with limit assigned charge
747 states to a range of 1; compound filters based on Quality Score > 70. The .cef converted data
748 represents each peak in the mass-to-charge (*m/z*) dimension as a single, discrete peak in the
749 mass spectrum, reducing data size and the grouping of adducts for every molecular feature.
750 Following, the table of putative metabolic features, along with their relative intensities,
751 was then aligned with Agilent Mass Profiler Professional - MPP (version 15.1). In brief, feature
752 alignment allowed mass tolerances of 0.003 AMU or 20 ppm and retention time tolerance of
753 0.3 min or 3%; minimum absolute abundance 10.000 counts; minimum number of ions 3;
754 multiple charge states forbidden. The final feature table was also filtered to retain only
755 features that appear in 75% of replicates of at least one condition and submitted to MS1
756 feature annotation against the Metabolite and Tandem MS Database (METLIN) (v1233)[69] was
757 performed by Agilent MPP. Human Metabolome Database (HMDB) accession numbers were

758 also derived from METLIN, and compound classes were assigned based on the latest HMDB
759 release (v5.0)[70].
760 The resulting feature quantification table was processed in R (v4.4.1) using
761 RStudio/2024.09.1, applying an adapted protocol for blank removal, imputation, quantile
762 normalization, and log-transformation[71]. In brief, features with specific blank-to-sample ratios
763 and samples with abnormally low mean intensities were flagged as poor-quality and removed
764 from analysis. The remaining data were imputed to address missing values, in which a limit of
765 detection (LOD) threshold was established based on the minimum non-zero intensity in the
766 data. Values below this threshold were imputed to the LOD cutoff. Intensities were then
767 quantile-normalized using the normalize.quantiles function from the preprocessCore package
768 (v1.64.0) ref and subsequently $\log_2$ transformed with a pseudo-count (half of the minimum
769 positive value) to stabilize variance was applied. For multivariate analysis such as PCA, data
770 were also z-scored (mean-centering and unit-variance scaling).
771 Multivariate and statistical analyses were performed in R 4.4.1 using
772 RStudio/2023.06.1. First, the prcomp function was used for Principal Component Analysis
773 (PCA) for data visualization, detection of sample outliers, and overall sample similarity.
774 Volcano plots were done to statistically compare spent media before and after Kpn
775 inoculation. The significance of a molecular feature was based on the intensity differences, in
776 which the p-values were assessed by t-test (t.test function in R). The p-values were FDR-
777 corrected for multiple hypotheses testing using the Benjamini-Hochberg procedure (p.adjust
778 function in R with 'fdr' parameter). Significant metabolites were selected when their intensity
779 had a fold change > 0.5 and a corrected p-value < 0.05.
780 Lastly, the area under the curve from significant features was integrated using the MassHunter
781 Quantitative Analysis Software (Agilent, version 7.0) based on the accurate high-resolution
782 mass and RT of the reference analytes with the following parameters: signal threshold of
783 30,000; mass tolerances of 0.003 amu or 20 ppm; retention time tolerance of 0.5 min. All
784 metabolites annotated in this manuscript were assigned a Level 1 annotation according to the
785 Metabolomics Standards Initiative (MSI) classification system. This includes a match in
786 retention time using the same chromatographic system, accurate mass, and MS/MS
787 fragmentation pattern, ensuring unequivocal identification of the compounds.
788
789 <u>Proteomics</u>

790 For the differential abundance proteomics, cultures were grown anaerobically at °C to
791 mid log phase (OD600 = 0.5), washed once with PBS and snap frozen. Pellets were
792 resuspended in 2% SDS and incubated at 99 °C for 5 min.
793 TPP was performed as previously described[46,72]. In brief, *K. pneumoniae ompK*^{evo}
794 cultures were grown anaerobically at 37 °C overnight. Cells were then washed twice
795 with anaerobic PBS, resuspended in lysis buffer (50 ug/ml lysozyme, 1mM MgCl2,
796 cOmplete protease inhibitors, 0.25 U/ul benzonase in PBS) and lysed with 5 freeze-
797 thaw cycles. Crude lysates (protein concentrations normalized to 10 ug/ul) were
798 treated with filter-sterilized spent medium prepared from various *E. coli* strains as
799 described previously for 10 min at RT. Aliquots of treated lysates were then incubated
800 in 10 different temperatures for 3 min, followed by 3 min at RT and 5min on ice. NP-
801 40 was added to a final concentration of 0.8%, aggregates were removed by filtration
802 and soluble proteins were prepared for mass spec.
803 Proteins were prepared and digested as previously described[73,74]. Eluted peptides
804 were labelled with TMT16plex, for the differential abundance proteomics, and
805 TMT18plex, for the TPP experiment. Samples were then pooled (all samples of each
806 two adjacent temperatures for the TPP experiment) and pre-fractionated into 6
807 fractions under high pH conditions. Samples were then analyzed with liquid
808 chromatography coupled to tandem mass spectrometry, as previously described[46].
809 For the differential abundance proteomics, MS data were processed as previously
810 described[74]. Briefly, raw MS files were processed with isobarQuant[75] and the
811 identification of peptide and protein was performed with Mascot 1.0 (Matrix Science)
812 against a FASTA database of translated ORFs annotated in CP009208 modified to
813 include known contaminants and the reversed protein sequences.
814 For the TPP experiment, raw files were converted to mzML format using MSConvert
815 from ProteoWizard, using peak picking, 64-bit encoding and zlib compression, and
816 filtering for the 1000 most intense peaks. Files were then searched using MSFragger
817 (v4.0)[76] in FragPipe (21.1) against a FASTA database of translated ORFs annotated
818 in CP009208 containing common contaminants and reversed sequences.
819 Data analysis was performed using R. Proteins with at least one uniquely identified
820 peptide were kept for the analysis. For the differential abundance proteomics, protein
821 intensities across all strains were normalized using variance stabilization
822 normalization[77] and limma was used to assess the differential expression of proteins.
823 For the TPP experiment, protein intensities across all conditions within each

824 temperature were normalized as above and the abundance and thermal stability
825 scores were calculated as previously described [74,78]. To assess the significance of
826 abundance and thermal stability scores, limma was used [79].
827
828 **Supplementary material**
829 Extended Data Fig. 1 - Abundance of *K. pneumoniae* wild type in different community
830 compositions over 4 days.
831 Extended Data Fig. 2 – Change in ratios over time of *K. pneumoniae* competitors in presence
832 and absence of various communities.
833 Extended Data Fig. 3 – Selection coefficient of *K. pneumoniae ompK*^{evo} in different
834 microbiomes.
835 Extended Data Fig. 4 – Scatter plot of *K. pneumoniae ompK*^{evo} over *K. pneumoniae* wild type
836 ratios against taxon relative abundances in microbiome MB003 derived subcommunities.
837 Extended Data Fig. 5 – Box plot of taxon relative abundances between high fitness ratio and
838 low fitness ratio perturbation conditions.
839 Extended Data Fig. 6 – Ratio of *K. pneumoniae ompK*^{evo} over the wild type in presence of *E.*
840 *coli*^{MB003} over 40 generations of growth.
841 Extended Data Fig. 7 – Abundance of *E. coli* in native stool samples from MB001-MB010.
842 Extended Data Fig. 8 – Protein abundance changes in *K. pneumoniae ompK*^{evo} versus *K.*
843 *pneumoniae* wild type.
844 Extended Data Fig. 9 – Structure analysis of GlyP.
845 Extended Data Fig. 10 – Growth rates of *K. pneumoniae wild type, K. pneumoniae ompK*^{mut}
846 *and K. pneumoniae ompK*^{evo} in various *E. coli*-spent media.
847 Extended Data Fig. 11 – Abundance of glycerol-containing metabolites in *E. coli*-spent media
848 in presence or absence of *K. pneumoniae*.
849
850 **Data availability**
851 Sequencing data of the K. pneumoniae isolates has been deposited in the European
852 Nucleotide Archive (ENA) at EMBL-EBI under accession number PRJEB110171. *K. pneumoniae*
853 CC258 genomes used in the ancestral reconstruction analysis are publicly-available with
854 accessions included in the Microreact project: https://microreact.org/project/kp-cc258. The
855 mass spectrometry proteomics data have been deposited to the ProteomeXchange

Consortium via the PRIDE partner repository with the dataset identifier PXD075097. The metabolomics data is available in the MetaboLights database (https://www.ebi.ac.uk/metabolights/) under accession number MTBLS7388.

Acknowledgements

We thank A. Mateus for assistance with proteomic analyses, D. Hazenbrink and C. G. P. Voogdt for assistance with subcommunity enrichments of fecal microbiomes, Maria I. Keller for DNA extraction of fecal microbiome samples and S. Giri for valuable discussions throughout the project. We also thank the EMBL core facilities for Genomics, Metabolomics, Proteomics, Flow Cytometry and Microbial Automation & Culturomics for their extended support throughout the project.

Author contribution

M.K. and A.T. acquired funding and conceptualized the study. M.K., S.G-S., L.M, D.P., V.C. and D.M.S. performed the experiments. S.D., J.L.C.W. and N.K. performed the computational analysis. G.F., M.Z., M.M. and A.T. supervised this study. M.K., L.M., D.P., S.D. and N.K. visualized the data and generated the figures. M.K. and A.T. wrote the original draft of the manuscript. All authors discussed the results and reviewed and edited the final version of the manuscript.

Funding.

This work was supported by a postdoctoral research grant of the Swedish research council (2019-00666) to M.K., the ERC consolidator grant uCARE (ID 819454), EMBL core funding and an Infection Biology Transversal Theme Synergy Grant to A.T.

Conflict of interest

The authors declare no conflict of interest.

References

1 Teillant, A., Gandra, S., Barter, D., Morgan, D. J. & Laxminarayan, R. Potential burden of antibiotic resistance on surgery and cancer chemotherapy antibiotic prophylaxis in the

USA: a literature review and modelling study. *Lancet Infect Dis* **15**, 1429-1437 (2015). https://doi.org:10.1016/S1473-3099(15)00270-4

2 Antimicrobial Resistance, C. Global burden of bacterial antimicrobial resistance in 2019: a systematic analysis. *Lancet* **399**, 629-655 (2022). https://doi.org:10.1016/S0140-6736(21)02724-0

3 Collaborators, G. B. D. A. R. Global burden of bacterial antimicrobial resistance 1990-2021: a systematic analysis with forecasts to 2050. *Lancet* **404**, 1199-1226 (2024). https://doi.org:10.1016/S0140-6736(24)01867-1

4 Farha, M. A., Tu, M. M. & Brown, E. D. Important challenges to finding new leads for new antibiotics. *Curr Opin Microbiol* **83**, 102562 (2025). https://doi.org:10.1016/j.mib.2024.102562

5 Hutchings, M. I., Truman, A. W. & Wilkinson, B. Antibiotics: past, present and future. *Curr Opin Microbiol* **51**, 72-80 (2019). https://doi.org:10.1016/j.mib.2019.10.008

6 Ross, J. D. C. *et al.* Oral gepotidacin for the treatment of uncomplicated urogenital gonorrhoea (EAGLE-1): a phase 3 randomised, open-label, non-inferiority, multicentre study. *Lancet* **405**, 1608-1620 (2025). https://doi.org:10.1016/S0140-6736(25)00628-2

7 Imai, Y. *et al.* A new antibiotic selectively kills Gram-negative pathogens. *Nature* **576**, 459-464 (2019). https://doi.org:10.1038/s41586-019-1791-1

8 Pahil, K. S. *et al.* Author Correction: A new antibiotic traps lipopolysaccharide in its intermembrane transporter. *Nature* **631**, E18 (2024). https://doi.org:10.1038/s41586-024-07645-0

9 Zampaloni, C. *et al.* Author Correction: A novel antibiotic class targeting the lipopolysaccharide transporter. *Nature* **631**, E17 (2024). https://doi.org:10.1038/s41586-024-07641-4

10 Theuretzbacher, U. *et al.* Critical analysis of antibacterial agents in clinical development. *Nat Rev Microbiol* **18**, 286-298 (2020). https://doi.org:10.1038/s41579-020-0340-0

11 Brochado, A. R. *et al.* Species-specific activity of antibacterial drug combinations. *Nature* **559**, 259-263 (2018). https://doi.org:10.1038/s41586-018-0278-9

12 Cacace, E. *et al.* Systematic analysis of drug combinations against Gram-positive bacteria. *Nat Microbiol* **8**, 2196-2212 (2023). https://doi.org:10.1038/s41564-023-01486-9

13 Lehar, S. M. *et al.* Novel antibody-antibiotic conjugate eliminates intracellular S. aureus. *Nature* **527**, 323-328 (2015). https://doi.org:10.1038/nature16057

14 Tooke, C. L. *et al.* beta-Lactamases and beta-Lactamase Inhibitors in the 21st Century. *J Mol Biol* **431**, 3472-3500 (2019). https://doi.org:10.1016/j.jmb.2019.04.002

15 Imamovic, L. & Sommer, M. O. Use of collateral sensitivity networks to design drug cycling protocols that avoid resistance development. *Sci Transl Med* **5**, 204ra132 (2013). https://doi.org:10.1126/scitranslmed.3006609

16 Baym, M., Stone, L. K. & Kishony, R. Multidrug evolutionary strategies to reverse antibiotic resistance. *Science* **351**, aad3292 (2016). https://doi.org:10.1126/science.aad3292

17 Kim, S., Lieberman, T. D. & Kishony, R. Alternating antibiotic treatments constrain evolutionary paths to multidrug resistance. *Proc Natl Acad Sci U S A* **111**, 14494-14499 (2014). https://doi.org:10.1073/pnas.1409800111

18 Lazar, V. *et al.* Bacterial evolution of antibiotic hypersensitivity. *Mol Syst Biol* **9**, 700 (2013). https://doi.org:10.1038/msb.2013.57

19 Imamovic, L. *et al.* Drug-Driven Phenotypic Convergence Supports Rational Treatment Strategies of Chronic Infections. *Cell* **172**, 121-134 e114 (2018). https://doi.org:10.1016/j.cell.2017.12.012

20 Sakenova, N. *et al.* Systematic mapping of antibiotic cross-resistance and collateral sensitivity with chemical genetics. *Nat Microbiol* **10**, 202-216 (2025). https://doi.org:10.1038/s41564-024-01857-w

21 Andersson, D. I. & Levin, B. R. The biological cost of antibiotic resistance. *Curr Opin Microbiol* **2**, 489-493 (1999). https://doi.org:10.1016/s1369-5274(99)00005-3

22 Dunai, A. *et al.* Rapid decline of bacterial drug-resistance in an antibiotic-free environment through phenotypic reversion. *Elife* **8** (2019). https://doi.org:10.7554/eLife.47088

23 Norstrom, T., Lannergard, J. & Hughes, D. Genetic and phenotypic identification of fusidic acid-resistant mutants with the small-colony-variant phenotype in Staphylococcus aureus. *Antimicrob Agents Chemother* **51**, 4438-4446 (2007). https://doi.org:10.1128/AAC.00328-07

24 Spragge, F. *et al.* Microbiome diversity protects against pathogens by nutrient blocking. *Science* **382**, eadj3502 (2023). https://doi.org:10.1126/science.adj3502

25 Carlet, J. The gut is the epicentre of antibiotic resistance. *Antimicrob Resist Infect Control* **1**, 39 (2012). https://doi.org:10.1186/2047-2994-1-39

26 Raymond, F. *et al.* Culture-enriched human gut microbiomes reveal core and accessory resistance genes. *Microbiome* **7**, 56 (2019). https://doi.org:10.1186/s40168-019-0669-7

27 Wyres, K. L. *et al.* Genomic surveillance of antimicrobial resistant bacterial colonisation and infection in intensive care patients. *BMC Infect Dis* **21**, 683 (2021). https://doi.org:10.1186/s12879-021-06386-z

28 Garcia-Bayona, L. & Comstock, L. E. Bacterial antagonism in host-associated microbial communities. *Science* **361** (2018). https://doi.org:10.1126/science.aat2456

29 Culp, E. J. & Goodman, A. L. Cross-feeding in the gut microbiome: Ecology and mechanisms. *Cell Host Microbe* **31**, 485-499 (2023). https://doi.org:10.1016/j.chom.2023.03.016

30 Gordo, I., Perfeito, L. & Sousa, A. Fitness effects of mutations in bacteria. *J Mol Microbiol Biotechnol* **21**, 20-35 (2011). https://doi.org:10.1159/000332747

31 Bertagnolio, S. *et al.* WHO global research priorities for antimicrobial resistance in human health. *Lancet Microbe* **5**, 100902 (2024). https://doi.org:10.1016/S2666-5247(24)00134-4

32 Navon-Venezia, S., Kondratyeva, K. & Carattoli, A. Klebsiella pneumoniae: a major worldwide source and shuttle for antibiotic resistance. *FEMS Microbiol Rev* **41**, 252-275 (2017). https://doi.org:10.1093/femsre/fux013

33 Raffelsberger, N. *et al.* Gastrointestinal carriage of Klebsiella pneumoniae in a general adult population: a cross-sectional study of risk factors and bacterial genomic diversity. *Gut Microbes* **13**, 1939599 (2021). https://doi.org:10.1080/19490976.2021.1939599

34 Wong, J. L. C. *et al.* OmpK36-mediated Carbapenem resistance attenuates ST258 Klebsiella pneumoniae in vivo. *Nat Commun* **10**, 3957 (2019). https://doi.org:10.1038/s41467-019-11756-y

35 Garcia-Santamarina, S. *et al.* Emergence of community behaviors in the gut microbiota upon drug treatment. *Cell* **187**, 6346-6357 e6320 (2024). https://doi.org:10.1016/j.cell.2024.08.037

36 Griesshammer, A. *et al.* Non-antibiotics disrupt colonization resistance against enteropathogens. *Nature* **644**, 497-505 (2025). https://doi.org:10.1038/s41586-025-09217-2

37 Ruscheweyh, H. J. *et al.* mOTUs: Profiling Taxonomic Composition, Transcriptional Activity and Strain Populations of Microbial Communities. *Curr Protoc* **1**, e218 (2021). https://doi.org:10.1002/cpz1.218

38 Tenaillon, O., Skurnik, D., Picard, B. & Denamur, E. The population genetics of commensal Escherichia coli. *Nat Rev Microbiol* **8**, 207-217 (2010). https://doi.org:10.1038/nrmicro2298

39 Galardini, M. *et al.* Phenotype inference in an *Escherichia coli* strain panel. *Elife* **6** (2017). https://doi.org:10.7554/eLife.31035

40 Andersen, C., Krones, D., Ulmke, C., Schmid, K. & Benz, R. The porin RafY encoded by the raffinose plasmid pRSD2 of Escherichia coli forms a general diffusion pore and not a carbohydrate-specific porin. *Eur J Biochem* **254**, 679-684 (1998). https://doi.org:10.1046/j.1432-1327.1998.2540679.x

41 Ulmke, C., Lengeler, J. W. & Schmid, K. Identification of a new porin, RafY, encoded by raffinose plasmid pRSD2 of Escherichia coli. *J Bacteriol* **179**, 5783-5788 (1997). https://doi.org:10.1128/jb.179.18.5783-5788.1997

42 Nikaido, H. Molecular basis of bacterial outer membrane permeability revisited. *Microbiology and molecular biology reviews : MMBR* **67**, 593-656 (2003).

43 Dunstan, R. A. *et al.* Epitopes in the capsular polysaccharide and the porin OmpK36 receptors are required for bacteriophage infection of Klebsiella pneumoniae. *Cell Rep* **42**, 112551 (2023). https://doi.org:10.1016/j.celrep.2023.112551

44 Low, W. W. *et al.* Mating pair stabilization mediates bacterial conjugation species specificity. *Nat Microbiol* **7**, 1016-1027 (2022). https://doi.org:10.1038/s41564-022-01146-4

45 Savitski, M. M. *et al.* Tracking cancer drugs in living cells by thermal profiling of the proteome. *Science* **346**, 1255784 (2014). https://doi.org:10.1126/science.1255784

46 Mateus, A. *et al.* Thermal proteome profiling in bacteria: probing protein state *in vivo*. *Mol Syst Biol* **14**, e8242 (2018). https://doi.org:10.15252/msb.20188242

47 Eberl, C. *et al. E. coli* enhance colonization resistance against *Salmonella* Typhimurium by competing for galactitol, a context-dependent limiting carbon source. *Cell host & microbe* **29**, 1680-1692 e1687 (2021). https://doi.org:10.1016/j.chom.2021.09.004

48 Osbelt, L. *et al.* Klebsiella oxytoca causes colonization resistance against multidrug-resistant K. pneumoniae in the gut via cooperative carbohydrate competition. *Cell Host Microbe* **29**, 1663-1679 e1667 (2021). https://doi.org:10.1016/j.chom.2021.09.003

49 Oliveira, R. A. *et al.* Klebsiella michiganensis transmission enhances resistance to Enterobacteriaceae gut invasion by nutrition competition. *Nat Microbiol* **5**, 630-641 (2020). https://doi.org:10.1038/s41564-019-0658-4

50 Woelfel, S., Silva, M. S. & Stecher, B. Intestinal colonization resistance in the context of environmental, host, and microbial determinants. *Cell Host Microbe* **32**, 820-836 (2024). https://doi.org:10.1016/j.chom.2024.05.002

51 Almasi, E. D. H. *et al.* Klebsiella oxytoca facilitates microbiome recovery via antibiotic degradation and restores colonization resistance in a diet-dependent manner. *Nat Commun* **16**, 551 (2025). https://doi.org:10.1038/s41467-024-55800-y

52 Forage, R. G. & Foster, M. A. Glycerol fermentation in Klebsiella pneumoniae: functions of the coenzyme B12-dependent glycerol and diol dehydratases. *J Bacteriol* **149**, 413-419 (1982). https://doi.org:10.1128/jb.149.2.413-419.1982

53 Raynaud, C., Sarcabal, P., Meynial-Salles, I., Croux, C. & Soucaille, P. Molecular characterization of the 1,3-propanediol (1,3-PD) operon of Clostridium butyricum. *Proc Natl Acad Sci U S A* **100**, 5010-5015 (2003). https://doi.org:10.1073/pnas.0734105100

54 Guo, Y. *et al.* 1,3-Propanediol production by a newly isolated strain, Clostridium perfringens GYL. *Bioresour Technol* **233**, 406-412 (2017). https://doi.org:10.1016/j.biortech.2017.02.116

55 Murali, A., Bhargava, A. & Wright, E. S. IDTAXA: a novel approach for accurate taxonomic classification of microbiome sequences. *Microbiome* **6**, 140 (2018). https://doi.org:10.1186/s40168-018-0521-5

56 Dmitrijeva, M. *et al.* The mOTUs online database provides web-accessible genomic context to taxonomic profiling of microbial communities. *Nucleic Acids Res* **53**, D797-D805 (2025). https://doi.org:10.1093/nar/gkae1004

57 Datsenko, K. A. & Wanner, B. L. One-step inactivation of chromosomal genes in Escherichia coli K-12 using PCR products. *Proc Natl Acad Sci U S A* **97**, 6640-6645 (2000). https://doi.org:10.1073/pnas.120163297

58 Datta, S., Costantino, N. & Court, D. L. A set of recombineering plasmids for gram-negative bacteria. *Gene* **379**, 109-115 (2006). https://doi.org:10.1016/j.gene.2006.04.018

59 Argimon, S. *et al.* Rapid Genomic Characterization and Global Surveillance of Klebsiella Using Pathogenwatch. *Clin Infect Dis* **73**, S325-S335 (2021). https://doi.org:10.1093/cid/ciab784

60 Danecek, P. *et al.* Twelve years of SAMtools and BCFtools. *Gigascience* **10** (2021). https://doi.org:10.1093/gigascience/giab008

61 Croucher, N. J. *et al.* Rapid phylogenetic analysis of large samples of recombinant bacterial whole genome sequences using Gubbins. *Nucleic Acids Res* **43**, e15 (2015). https://doi.org:10.1093/nar/gku1196

62 Kozlov, A. M., Darriba, D., Flouri, T., Morel, B. & Stamatakis, A. RAxML-NG: a fast, scalable and user-friendly tool for maximum likelihood phylogenetic inference. *Bioinformatics* **35**, 4453-4455 (2019). https://doi.org:10.1093/bioinformatics/btz305

63 Lam, M. M. C. *et al.* A genomic surveillance framework and genotyping tool for Klebsiella pneumoniae and its related species complex. *Nat Commun* **12**, 4188 (2021). https://doi.org:10.1038/s41467-021-24448-3

64 Camacho, C. *et al.* BLAST+: architecture and applications. *BMC Bioinformatics* **10**, 421 (2009). https://doi.org:10.1186/1471-2105-10-421

65 Gouy, M., Tannier, E., Comte, N. & Parsons, D. P. Seaview Version 5: A Multiplatform Software for Multiple Sequence Alignment, Molecular Phylogenetic Analyses, and Tree Reconciliation. *Methods Mol Biol* **2231**, 241-260 (2021). https://doi.org:10.1007/978-1-0716-1036-7_15

66 Argimon, S. *et al.* Microreact: visualizing and sharing data for genomic epidemiology and phylogeography. *Microb Genom* **2**, e000093 (2016). https://doi.org:10.1099/mgen.0.000093

67 Carver, T. J. *et al.* ACT: the Artemis Comparison Tool. *Bioinformatics* **21**, 3422-3423 (2005). https://doi.org:10.1093/bioinformatics/bti553

68 Assefa, S., Keane, T. M., Otto, T. D., Newbold, C. & Berriman, M. ABACAS: algorithm-based automatic contiguation of assembled sequences. *Bioinformatics* **25**, 1968-1969 (2009). https://doi.org:10.1093/bioinformatics/btp347

69 Montenegro-Burke, J. R., Guijas, C. & Siuzdak, G. METLIN: A Tandem Mass Spectral Library of Standards. *Methods Mol Biol* **2104**, 149-163 (2020). https://doi.org:10.1007/978-1-0716-0239-3_9

70 Wishart, D. S. *et al.* HMDB 5.0: the Human Metabolome Database for 2022. *Nucleic Acids Res* **50**, D622-D631 (2022). https://doi.org:10.1093/nar/gkab1062

71 Dricot, C. E. M. K. *et al.* Vitamin B₂ Production by Vaginal Lactobacilli Promotes Symbiosis. *bioRxiv*, 2025.2010.2028.684342 (2025). https://doi.org:10.1101/2025.10.28.684342

72 Klunemann, M. *et al.* Bioaccumulation of therapeutic drugs by human gut bacteria. *Nature* **597**, 533-538 (2021). https://doi.org:10.1038/s41586-021-03891-8

73 Hughes, C. S. *et al.* Single-pot, solid-phase-enhanced sample preparation for proteomics experiments. *Nat Protoc* **14**, 68-85 (2019). https://doi.org:10.1038/s41596-018-0082-x

74 Mateus, A. *et al.* The functional proteome landscape of Escherichia coli. *Nature* **588**, 473-478 (2020). https://doi.org:10.1038/s41586-020-3002-5

75 Franken, H. *et al.* Thermal proteome profiling for unbiased identification of direct and indirect drug targets using multiplexed quantitative mass spectrometry. *Nat Protoc* **10**, 1567-1593 (2015). https://doi.org:10.1038/nprot.2015.101

76 Kong, A. T., Leprevost, F. V., Avtonomov, D. M., Mellacheruvu, D. & Nesvizhskii, A. I. MSFragger: ultrafast and comprehensive peptide identification in mass spectrometry-based proteomics. *Nat Methods* **14**, 513-520 (2017). https://doi.org:10.1038/nmeth.4256

77 Huber, W., von Heydebreck, A., Sultmann, H., Poustka, A. & Vingron, M. Variance stabilization applied to microarray data calibration and to the quantification of differential expression. *Bioinformatics* **18 Suppl 1**, S96-104 (2002). https://doi.org:10.1093/bioinformatics/18.suppl_1.s96

78 Becher, I. *et al.* Pervasive Protein Thermal Stability Variation during the Cell Cycle. *Cell* **173**, 1495-1507 e1418 (2018). https://doi.org:10.1016/j.cell.2018.03.053

79 Ritchie, M. E. *et al.* limma powers differential expression analyses for RNA-sequencing and microarray studies. *Nucleic Acids Res* **43**, e47 (2015). https://doi.org:10.1093/nar/gkv007

1111 Figure Legends

1112 **Figure 1 – A sensitive method for identifying specific microbiotas that (counter-)select for**
1113 **an antibiotic resistant *K. pneumoniae* mutant. a,** Conventional methods to determine
1114 bacterial fitness *in vitro*. Fitness is measured by determining the lag time, exponential growth
1115 rate and maximum yield of an axenically grown culture, or by competing two differently
1116 tagged isogenic strains over time to determine their change in ratios, and thereby the
1117 selection coefficient. **b,** Schematic representation of factors influencing bacterial fitness in
1118 complex communities. **c,** Mutations present in the *K. pneumoniae* porin mutant. *ompK35*
1119 carries a frameshift mutation resulting in a premature stop after 66 amino acids causing a
1120 complete loss of function. *ompK*36 carries a series of clinically prevalent mutations including
1121 a GD-insertion resulting in a restriction of the pore diameter. **d,** Preparation of stool-derived
1122 microbial communities MB001 to MB010. Fecal samples of healthy human adults were mixed
1123 1:1 with PBS and diluted in mGAM broth, passaged anaerobically for 3 days in fresh medium
1124 and cryopreserved in presence of 12.5% glycerol. **e,** Preparation of the synthetic community
1125 SPP21. Overnight cultures of 21 prevalent gut bacterial species mixed at equimolar ratios. The
1126 synthetic community was grown overnight and cryopreserved in presence of 12.5% glycerol.
1127 **f,** Experimental setup of the competition experiment between various antibiotic-resistant *K.*
1128 *pneumoniae* strains in presence of different human gut microbiomes. Competitions were
1129 performed in 96 deep-well plates with daily passing over 3-4 days under anaerobic conditions
1130 with the indicated experimental parameters. Maturation of the fluorescent proteins, PFA-
1131 fixation and readout using flow cytometry were performed aerobically. **g,** Selection
1132 coefficients of *K. pneumoniae ompK35/ompK36* mutant (annotated as *K. pneumoniae*
1133 $ompK^{mut}$) with or without OXA48 or KPC-2 compared to an isogenic wildtype strain in absence
1134 (mGAM) or presence of 10 different fecal or synthetic microbiomes. All competitions were
1135 performed in a minimum of 5 replicates per marker combination, and all resistant mutant
1136 were competed against the wild type with GFP and RFP (with the mutant carrying the
1137 corresponding complementary marker). The GFP or RFP associated fitness cost was
1138 determined in a wildtype versus wildtype competition and used for subsequent correction of
1139 selection coefficients (see methods). Center lines show the medians; box limits indicate the
1140 25th and 75th percentiles; whiskers extend 1.5 times the interquartile range from the 25th
1141 and 75th percentiles, data points are plotted as dots. **h,** Change in ratio of $ompK^{mut}$ over *K.*

1142 *pneumoniae* wildtype in presence of MB003 over 4 days. Colors indicate the marker carried
1143 by the porin mutant. **i,** Change in ratio of *K. pneumoniae ompK*^{evo} over the wildtype in
1144 presence of MB003 over 4 days. Colors indicate if the evolved mutant was isolated from the
1145 GFP- or RFP-tagged lineage of *ompK*^{mut} **j,** Selection coefficient of seven *K. pneumoniae ompK*^{evo}
1146 endpoint clones over the wildtype in presence of MB003. The selection coefficients were
1147 corrected for the marker cost determined by the wildtype-wildtype competition in presence
1148 of MB003. Colors as in panel **i**.
1149
1150 **Figure 2 – Identification of Microbiome MB003 community members driving the enrichment**
1151 **of *K. pneumoniae ompK*^{evo}. a,** Composition, Shannon diversity and mOTU richness of the fecal
1152 derived communities MB001-MB010 based on metagenomic analysis (see methods). **b,** Ratio
1153 of *K. pneumoniae ompK*^{evo} over the wildtype after one day of co-culture in different MB003-
1154 derived subcommunities. The subcommunities were generated by daily passaging of MB003
1155 under various selective conditions for 3 days. The data points in the upper panel (n = 4
1156 replicates, error bars represent standard deviation) correspond to relative abundance of *K.*
1157 *pneumoniae ompK*^{evo} over the wildtype after passaging a 1:1 mixture in the subcommunities
1158 for 24hours (secondary y axis). The lower panel shows the microbial composition based on
1159 16S rRNA sequencing. *Escherichia* abundance is accentuated with a black outline.
1160
1161 **Figure 3 – The selective advantage of *K. pneumoniae ompK*^{evo} is driven by many *E. coli* strains**
1162 **and depends on higher-order interactions with other gut bacteria. a,** Selective advantage of
1163 *K. pneumoniae ompK*^{evo} over the wildtype in presence of different *E. coli* strains. The
1164 competitions were performed in the presence of each *E. coli* strain individually (triple
1165 competitions). Data points (primary y-axis) represent the average selection coefficient of *K.*
1166 *pneumoniae ompK*^{evo} over the wildtype of four replicates. Error bars represent the standard
1167 deviation. The stacked bars (secondary y-axis) represent abundance of the indicated strains
1168 at the end point of the competition experiment as determined by flow cytometry. Arrows
1169 above bars indicate *E. coli* strains that were isolated from the fecal microbiome MB003,
1170 MB001 and MB005 (left to right). **b,** Selective advantage of *K. pneumoniae ompK*^{evo} over the
1171 wildtype in presence of YFP-labelled *E. coli*^{MB003} and various fourth competitors. The
1172 competitions were performed in presence of each fourth competitor individually (quadruple
1173 competitions). Data representation as in panel **a**.

1174

1175 **Figure 4 – Mutations in a transcription factor in *K. pneumoniae ompK^{evo}* cause the fitness**
1176 **advantage in MB003, due to upregulation of a downstream porin. a,** Whole genome
1177 sequence analysis of seven *K. pneumoniae ompK^{evo}* mutants. All clones carry mutations in a
1178 LacI-type transcription factor resulting in premature stops, internal deletions or amino acid
1179 substitutions. The transcription factor is located upstream of a carbohydrate catabolic operon
1180 consisting of a permease, a hydrolase and an additional porin. The labels indicate the locus
1181 tags according to reference genome CP009208. **b,** Proteome abundance changes induced by
1182 acquisition of a *glyR* mutation in *K. pneumoniae ompK^{mut}*. The wildtype and evolved porin
1183 mutant carrying a T60P substitution in the LacI-type transcription factor were grown for 16
1184 hours in mGAM under anaerobic conditions and subjected to mass spectrometry. All genes of
1185 the carbohydrate catabolic operon are upregulated in the *glyR* T60P mutant. **c,** Selective
1186 advantage of various deletion mutants of the carbohydrate-catabolic operon in the *K.*
1187 *pneumoniae ompK^{evo}* background or in the wildtype background over the parental strain in
1188 presence of MB003. Box plots depicted as in Fig. 1g.

1189

1190 **Figure 5 – GlyP upregulation allows *K. pneumoniae* to benefit from glycerol containing**
1191 **compounds. a,** Growth curves of *K. pneumoniae* wild type, *K. pneumoniae ompK^{mut}* and *K.*
1192 *pneumoniae ompK^{evo}* in *E. coli^{MB003}* spent medium without supplements or **b,** with
1193 supplementation of 0.2% glucose. The spent medium was prepared by growing *E. coli^{MB003}*
1194 overnight in mGAM at 37 °C under anaerobic conditions and subsequent sterile filtration with
1195 a 0.22µM pore size filter. Lines represent average of four independent replicates, confidence
1196 intervals represent one standard deviation. **c,** Change in thermal stability of the proteome of
1197 *K. pneumoniae ompK^{evo}* compared to the wildtype in presence of *E. coli^{MB003}* spent medium
1198 (see methods). Three replicates of *K. pneumoniae ompK^{evo}* and *K. pneumoniae* wild type were
1199 grown anaerobically overnight in mGAM. Whole-cells lysates were treated with *E. coli^{MB003}*
1200 spent medium and subjected to thermal proteome profiling. Significant hits are indicated with
1201 red (destabilized) and blue (stabilized). Members of the carbohydrate catabolic operon
1202 described in **Fig. 4a** as well as the two strongest stabilized proteins are labelled. **d,**
1203 Metabolomics of *E. coli^{MB003}* spent medium before and after growth of *K. pneumoniae*
1204 *ompK^{evo}*. Compounds significantly enriched after growth of *K. pneumoniae ompK^{evo}* are
1205 coloured in blue, compounds significantly diminished are coloured in red. Glycerol-derivatives

1206 are labelled. **e**, Signal intensities for Glyceryl 5-hydroxydecanoate in spent media of seven
1207 different *E. coli* isolates and in mGAM before and after growth of *K pneumoniae ompK*^{evo}. All
1208 experiments were performed in six replicates. Box plots depicted as in Fig. 1g. **f**, Fitness of *K.*
1209 *pneumoniae ompK*^{mut} and *K. pneumoniae ompK*^{evo} compared to *K. pneumoniae* wildtype
1210 grown in different carbon sources. Competitions were performed in M9 minimal media
1211 supplemented with defined carbon sources as indicated. Box plots depicted as in Fig. 1g.
1212
1213 **Figure 6 - glyR T60P substitution is under conditional positive selection in clinical isolates of**
1214 ***K. pneumoniae*. a,** Number of base (state) changes inferred to have occurred across the
1215 phylogeny of 9214 CC258 isolates at each base position spanning the length of the *glyR*/*glyP*
1216 operons and with respect to the HS11286 reference genome. Base changes are colored by
1217 their effect on the protein sequence. **b**, Phylogenetic tree of 9214 CC258 isolates constructed
1218 after the removal of recombined regions from the alignment. Isolate nodes are colored pink
1219 if they possess a "C" at position 4366094 (with respect to the HS11286 reference),
1220 corresponding to amino acid position 60 within the LacI type TF. Metadata columns show
1221 whether the *glyR*, *ompK35* and *ompK36* genes are intact, truncated or absent, the presence
1222 or absence of an *ompK36* loop 3 insertion (GD or TD) and the ST of the genomes. Clades A and
1223 B are shown with additional resolution on the right-hand side. The scale bars represent the
1224 number of SNPs. An interactive vizualisation of this tree, together with additional metadata
1225 and genotypic data, is available via Microreact at https://microreact.org/project/kp-cc258.
1226
1227 **Extended Data Fig. 1: Abundance of *K. pneumoniae* wild type in different community**
1228 **compositions over 4 days.** Dark grey lines show the mean total abundance of the *K.*
1229 *pneumoniae* competitors in various communities. Light grey lines show the abundance in each
1230 replicate competition. Abundancies are determined by flow cytometry, where GFP^{+} and RFP^{+}
1231 cells represent *K. pneumoniae* and GFP^{-}/RFP^{-} events represent untagged community
1232 members. Competitions were passaged for 4 days in mGAM broth under anaerobic conditions
1233 at 37 °C with a daily dilution factor of 1:1000 corresponding to approximately 10 generations
1234 of growth per day.
1235
1236 **Extended Data Fig. 2: Change in ratios over time of *K. pneumoniae* competitors in presence**
1237 **and absence of various communities.** Green and red data points represent competitions

where the resistant mutant (*K. pneumoniae ompK*^{mut}*, ompK*^{mut} /pOXA48 *and ompK*^{mut} /KPC2) is tagged with GFP or RFP, respectively. Ratios were determined daily by flow cytometry. Competitions were passaged for 4 days in mGAM broth under anaerobic conditions at 37 °C with a daily dilution factor of 1:1000 corresponding to approximately 10 generations of growth per day.

Extended Data Fig. 3: Selection coefficient of *K. pneumoniae ompK*^{evo} in different microbiomes. *K. pneumoniae ompK*^{evo} GFP^{+} was competed with an RFP^{+} *K. pneumoniae* wild type over 4 days using the previously described competition setup in presence or absence of different microbial communities. Centre lines show the medians; box limits indicate the 25th and 75th percentiles as determined by R software; whiskers extend 1.5 times the interquartile range from the 25th and 75th percentiles, data points are plotted as dots. The experiment was performed with a minimum of four biological replicates.

Extended Data Fig. 4: Scatter plot of *K. pneumoniae ompK*^{evo} over *K. pneumoniae* wild type ratios against taxon relative abundances in microbiome MB003 derived subcommunities. Relative abundances of taxa are log10-scaled. Conditions are grouped into high and low fitness ratios. P-values were computed using a Pearson correlation test. Only genera with a relative abundance of at least 5% in at least one of the perturbation conditions are shown. See Extended Data Fig. 5 for a binarized depiction of the same data.

Extended Data Fig. 5: Box plot of taxon relative abundances between high fitness ratio and low fitness ratio perturbation conditions. Relative abundances of taxa are log10-scaled**.** Conditions are grouped into high and low fitness. P-values were computed using a Wilcoxon rank-sum test. Only genera with a relative abundance of at least 5% in at least one of the perturbation conditions are shown. See Extended Data Fig. 4 for a continuous depiction of the same data.

Extended Data Fig. 6: Ratio of *K. pneumoniae ompK*^{evo} over the wild type in presence of *E. coli*^{MB003} over 40 generations of growth.

Change in ratio of *K. pneumoniae ompK*^{mut} over *K. pneumoniae* wild type in presence of *E.coli*^{MB003} over 4 days of competition (see materials and methods). Each line represents a

1270 replicate competition and colours indicate the marker carried by the porin mutant (green =
1271 GFP, red = RFP)
1272
1273 **Extended Data Fig. 7: Abundance of *E. coli* in native stool samples from MB001-MB010.**
1274 Native stool samples for MB001-MB010 were Whole-Genome Shotgun (WGS) sequenced as
1275 described in Methods.
1276
1277 **Extended Data Fig. 8: Protein abundance changes in *K. pneumoniae ompK^{evo}* versus *K.*
1278 *pneumoniae* wild type.** The volcano plots show the up- or downregulated proteins in all seven
1279 isolated *K. pneumoniae ompK^{evo}* clones. Cells were grown over night in mGAM under
1280 anaerobic conditions and harvested after 20h for whole cell proteome analysis using mass
1281 spectrometry. Each strain was tested in three biological replicates.
1282
1283 **Extended Data Fig. 9: Structure analysis of GlyP**
1284 **a**, AlphaFold prediction of the *K. pneumoniae* porin upregulated in *K. pneumoniae ompK^{evo}*.
1285 The AlphaFold-predicted structure of the mature protein (signal peptide removed) is shown
1286 as a cartoon representation colored by pLDDT confidence scores. The ß-barrel core is
1287 predicted with high confidence. **b**, predicted aligned error (PAE) plot for the AlphaFold model.
1288 The PAE plot indicates high confidence in the relative positioning of residues withing the ß-
1289 barrel core, while increased predicted error is primarily associated with extracellular loop
1290 regions. The short cytoplasmic helix also displays reduced confidence, consistent with local
1291 flexibility and disorder. **c,** structure alignment of GlyP with RafY. UCSF ChimeraX structural
1292 superposition of the AlphaFold-predicted mature porin (blue) and RafY (grey) shows close
1293 alignment of the ß-barrel core with divergence in loop regions. The alignment produced a
1294 sequence alignment score of 1495.9 and an RMSD of 0.67Å over 312 pruned atom pairs (22.3Å
1295 across all aligned residues).
1296
1297 **Extended Data Fig. 10: Growth rates of *K. pneumoniae wild type, K. pneumoniae ompK^{mut}*
1298 *and K. pneumoniae ompK^{evo}* in various *E. coli*-spent media.**
1299 The spent media were prepared by growing different *E. coli* strains overnight in mGAM at 37
1300 ºC under anaerobic conditions and subsequent sterile filtration using a 0.22µM pore size filter.

1301 Lines represent average of four independent replicates, shades represent the standard
1302 deviation.
1303
1304
1305 **Extended Data Fig. 11: Abundance of glycerol-containing metabolites in *E. coli*-spent media**
1306 **in presence or absence of *K. pneumoniae*.**
1307 Absolute LC-MS signal intensities of (**a**) 1-O-hexadecyl-2-methyl-sn-glycerol (m/z 330.313) and
1308 (**b**) 1-O-(ß-D-glucopyranosyl)propane-1,2-diol (m/z 238.107) in culture supernatants of *E. coli*
1309 before and after growth of *K. pneumoniae ompK*^{evo}. A reduction in signal intensity indicates
1310 depletion of these metabolites. Values are based on 6 biological replicates.
1311

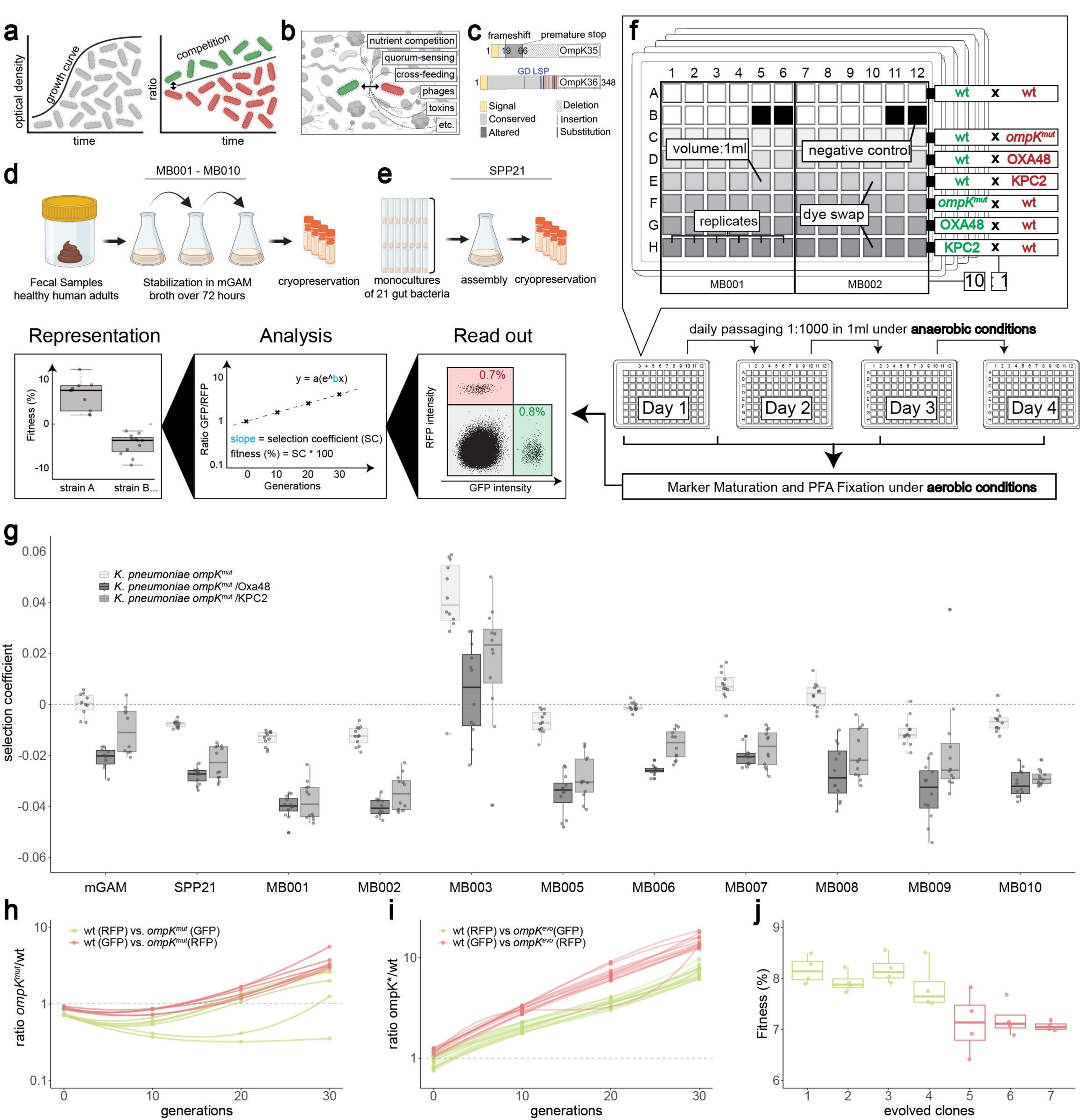
a
optical density
growth curve
time
competition
ratio
time
b
nutrient competition
quorum-sensing
cross-feeding
phages
toxins
etc.
c
frameshift
premature stop
OmpK35
GD LSP
OmpK36
Signal
Conserved
Altered
Deletion
Insertion
Substitution
d
MB001 - MB010
Fecal Samples healthy human adults
Stabilization in mGAM broth over 72 hours
cryopreservation
e
SPP21
monocultures of 21 gut bacteria
assembly
cryopreservation
f
volume:1ml
negative control
replicates
dye swap
wt x wt
wt x ompKmut
wt x OXA48
wt x KPC2
ompKmut x wt
OXA48 x wt
KPC2 x wt
MB001
MB002
daily passaging 1:1000 in 1ml under anaerobic conditions
Day 1
Day 2
Day 3
Day 4
Marker Maturation and PFA Fixation under aerobic conditions
Representation
Fitness (%)
strain A
strain B...
Analysis
Ratio GFP/RFP
y = a(e^bx)
slope = selection coefficient (SC)
fitness (%) = SC * 100
Generations
Read out
RFP intensity
GFP intensity
0.7%
0.8%
g
K. pneumoniae ompKmut
K. pneumoniae ompKmut /Oxa48
K. pneumoniae ompKmut /KPC2
selection coefficient
mGAM
SPP21
MB001
MB002
MB003
MB005
MB006
MB007
MB008
MB009
MB010
h
wt (RFP) vs. ompKmut (GFP)
wt (GFP) vs. ompKmut(RFP)
ratio ompKmut/wt
generations
i
wt (RFP) vs ompKevo(GFP)
wt (GFP) vs ompKevo (RFP)
ratio ompK*/wt
generations
j
Fitness (%)
evolved clones

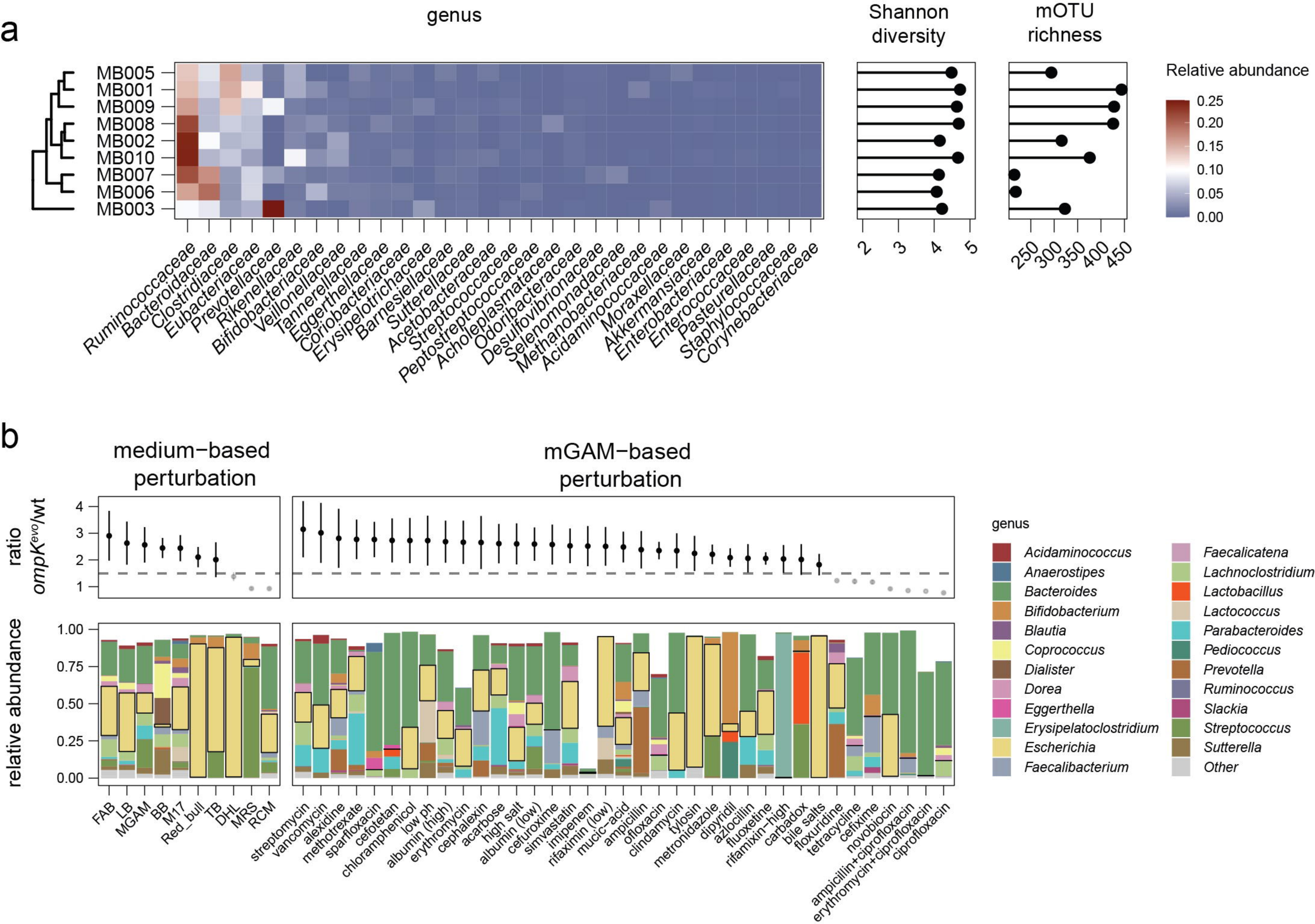
a
genus
Shannon diversity
mOTU richness
Relative abundance
0.25
0.20
0.15
0.10
0.05
0.00
MB005
MB001
MB009
MB008
MB002
MB010
MB007
MB006
MB003
Ruminococcaceae
Bacteroidaceae
Clostridiaceae
Eubacteriaceae
Prevotellaceae
Rikenellaceae
Bifidobacteriaceae
Veillonellaceae
Tannerellaceae
Eggerthellaceae
Coriobacteriaceae
Erysipelotrichaceae
Barnesiellaceae
Sutterellaceae
Acetobacteraceae
Streptococcaceae
Peptostreptococcaceae
Acholeplasmataceae
Odoribacteraceae
Desulfovibrionaceae
Selenomonadaceae
Methanobacteriaceae
Acidaminococcaceae
Moraxellaceae
Akkermansiaceae
Enterobacteriaceae
Enterococcaceae
Pasteurellaceae
Staphylococcaceae
Corynebacteriaceae
2
3
4
5
250
300
350
400
450
b
medium−based perturbation
mGAM−based perturbation
ratio
ompK^evo/wt
relative abundance
FAB
LB
MGAM
BB
M17
Red_bull
TB
DHL
MRS
RCM
streptomycin
vancomycin
alexidine
methotrexate
sparfloxacin
cefotetan
chloramphenicol
low ph
albumin (high)
erythromycin
cephalexin
acarbose
high salt
albumin (low)
cefuroxime
simvastatin
imipenem
rifaximin (low)
mucic−acid
ampicillin
ofloxacin
clindamycin
tylosin
metronidazole
dipyridil
azlocillin
fluoxetine
rifamixin−high
carbadox
bile salts
floxuridine
tetracycline
cefixime
novobiocin
ampicillin+ciprofloxacin
erythromycin+ciprofloxacin
ciprofloxacin
genus
Acidaminococcus
Anaerostipes
Bacteroides
Bifidobacterium
Blautia
Coprococcus
Dialister
Dorea
Eggerthella
Erysipelatoclostridium
Escherichia
Faecalibacterium
Faecalicatena
Lachnoclostridium
Lactobacillus
Lactococcus
Parabacteroides
Pediococcus
Prevotella
Ruminococcus
Slackia
Streptococcus
Sutterella
Other

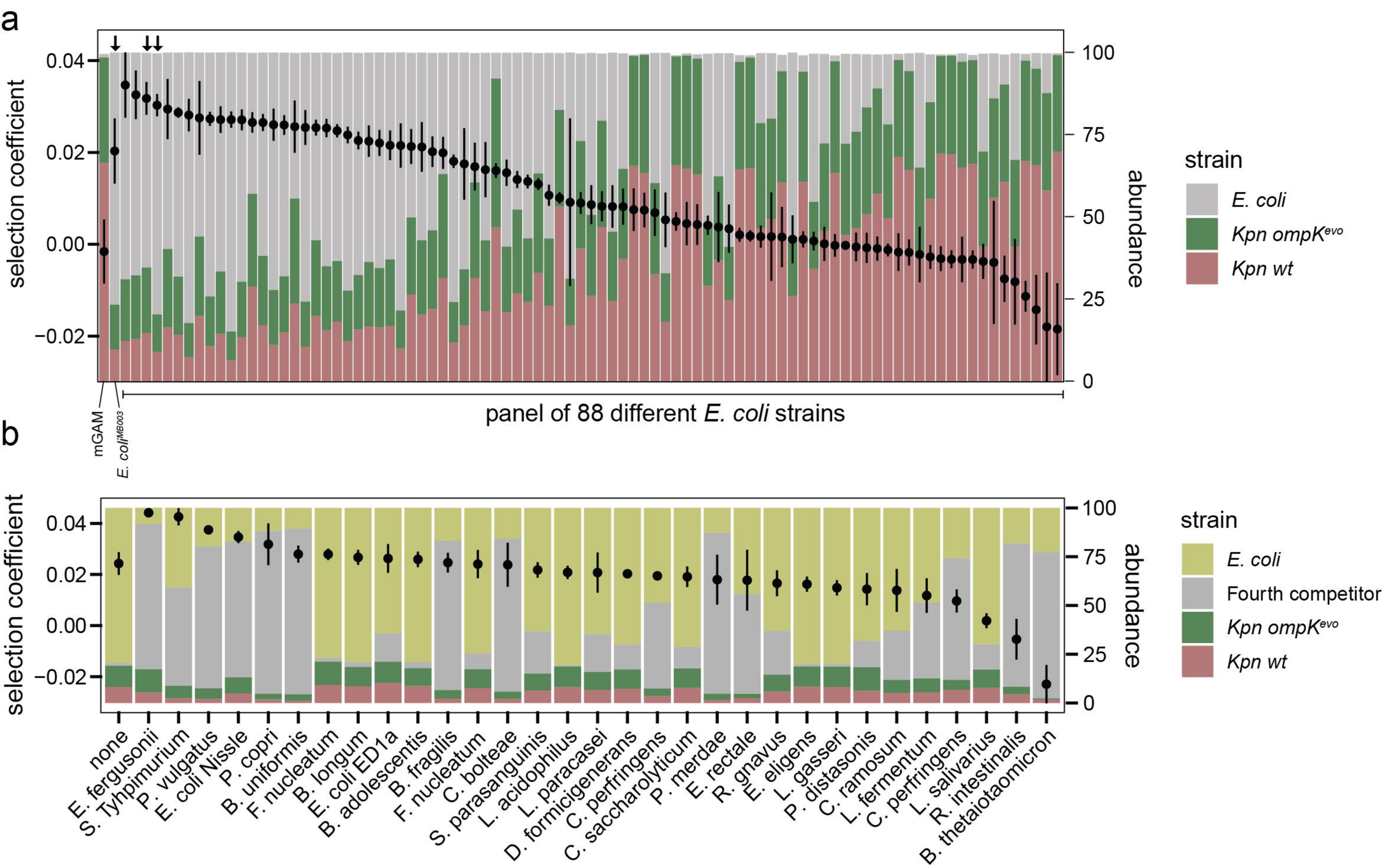
a
selection coefficient
0.04
0.02
0.00
−0.02
abundance
100
75
50
25
0
strain
E. coli
Kpn ompKevo
Kpn wt
mGAM
E. coliMB003
panel of 88 different E. coli strains
b
selection coefficient
0.04
0.02
0.00
−0.02
abundance
100
75
50
25
0
strain
E. coli
Fourth competitor
Kpn ompKevo
Kpn wt
none
E. fergusonii
S. Typhimurium
P. vulgatus
E. coli Nissle
P. copri
B. uniformis
F. nucleatum
B. longum
E. coli ED1a
B. adolescentis
B. fragilis
F. nucleatum
C. bolteae
S. parasanguinis
L. acidophilus
L. paracasei
D. formicigenerans
C. perfringens
C. saccharolyticum
P. merdae
E. rectale
R. gnavus
E. eligens
L. gasseri
P. distasonis
C. ramosum
L. fermentum
C. perfringens
L. salivarius
R. intestinalis
B. thetaiotaomicron

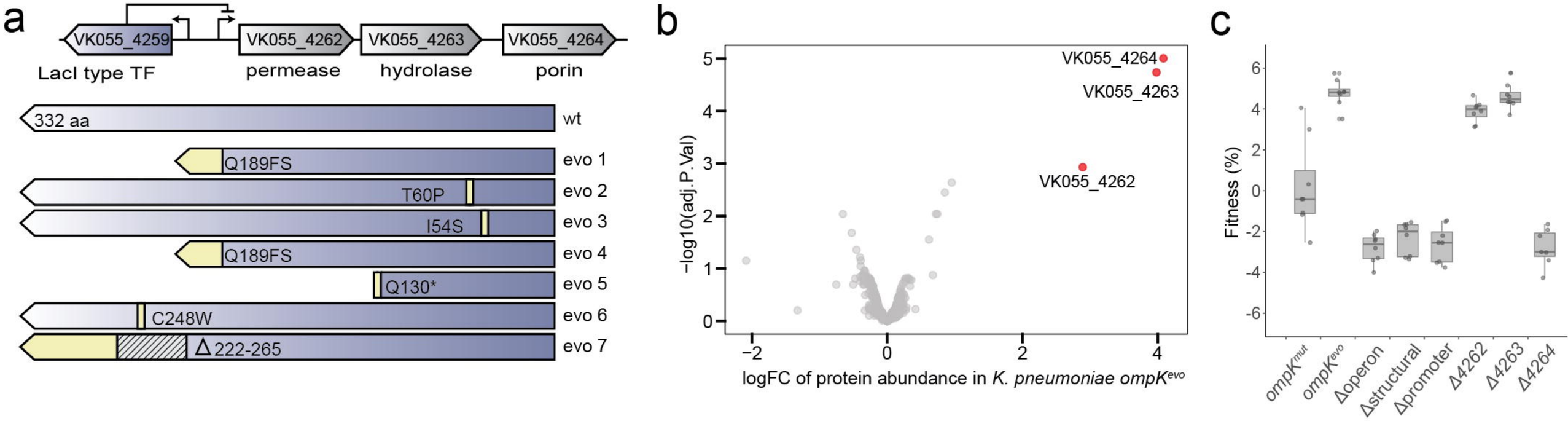
a
VK055_4259
VK055_4262
VK055_4263
VK055_4264
LacI type TF
permease
hydrolase
porin
332 aa
wt
Q189FS
evo 1
T60P
evo 2
I54S
evo 3
Q189FS
evo 4
Q130*
evo 5
C248W
evo 6
Δ222-265
evo 7
b
VK055_4264
VK055_4263
VK055_4262
−log10(adj.P.Val)
logFC of protein abundance in K. pneumoniae ompKevo
c
Fitness (%)
ompKmut
ompKevo
Δoperon
Δstructural
Δpromoter
Δ4262
Δ4263
Δ4264

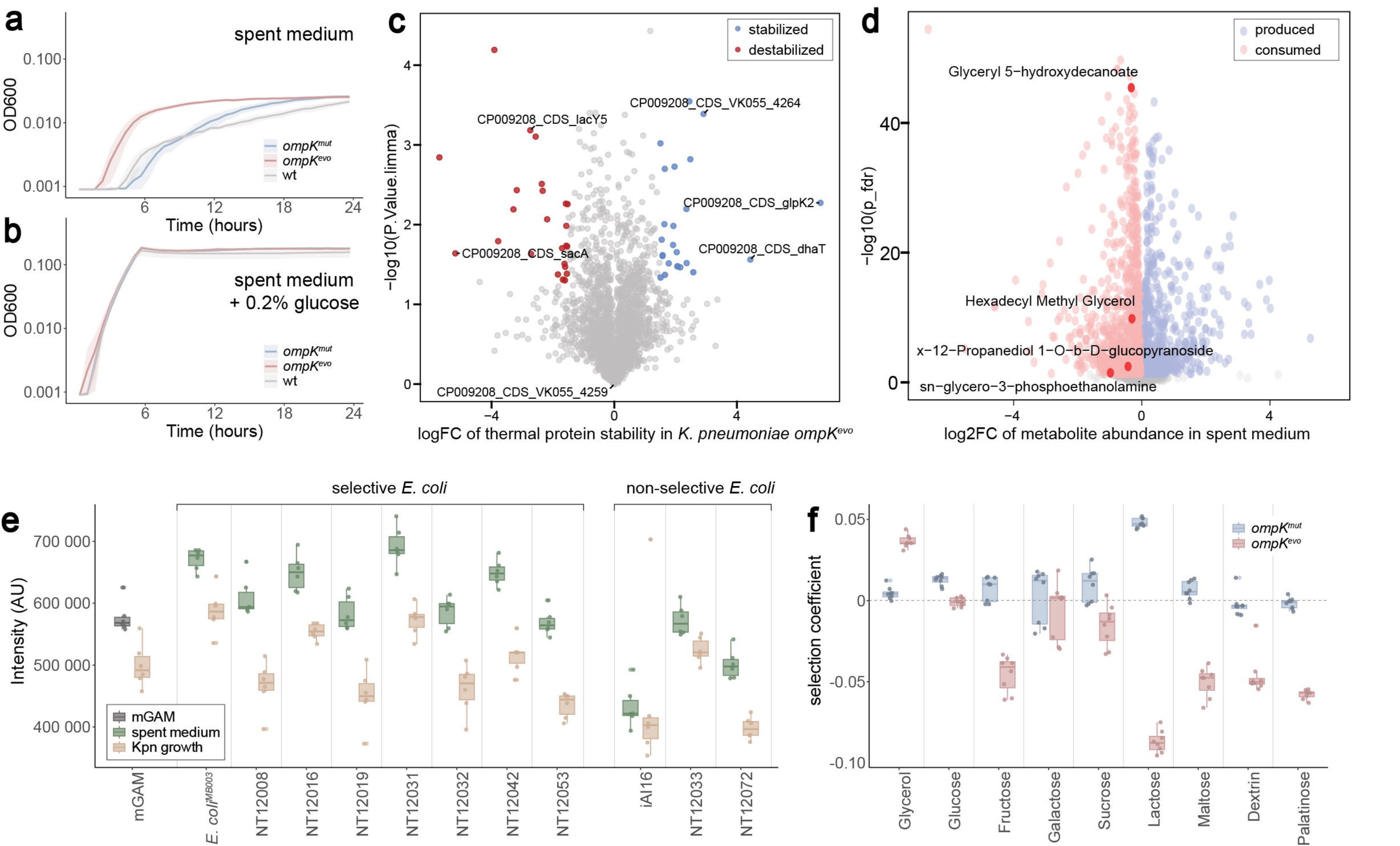
a
spent medium
OD600
0.100
0.010
0.001
ompKmut
ompKevo
wt
6
12
18
24
Time (hours)
b
spent medium
+ 0.2% glucose
OD600
0.100
0.010
0.001
ompKmut
ompKevo
wt
6
12
18
24
Time (hours)
c
stabilized
destabilized
−log10(P.Value.limma)
CP009208_CDS_VK055_4264
CP009208_CDS_lacY5
CP009208_CDS_glpK2
CP009208_CDS_dhaT
CP009208_CDS_sacA
CP009208_CDS_VK055_4259
logFC of thermal protein stability in K. pneumoniae ompKevo
d
produced
consumed
−log10(p_fdr)
Glyceryl 5−hydroxydecanoate
Hexadecyl Methyl Glycerol
x−12−Propanediol 1−O−b−D−glucopyranoside
sn−glycero−3−phosphoethanolamine
log2FC of metabolite abundance in spent medium
e
selective E. coli
non-selective E. coli
Intensity (AU)
700 000
600 000
500 000
400 000
mGAM
spent medium
Kpn growth
mGAM
E. coliMB003
NT12008
NT12016
NT12019
NT12031
NT12032
NT12042
NT12053
iAI16
NT12033
NT12072
f
selection coefficient
0.05
0
-0.05
-0.10
ompKmut
ompKevo
Glycerol
Glucose
Fructose
Galactose
Sucrose
Lactose
Maltose
Dextrin
Palatinose

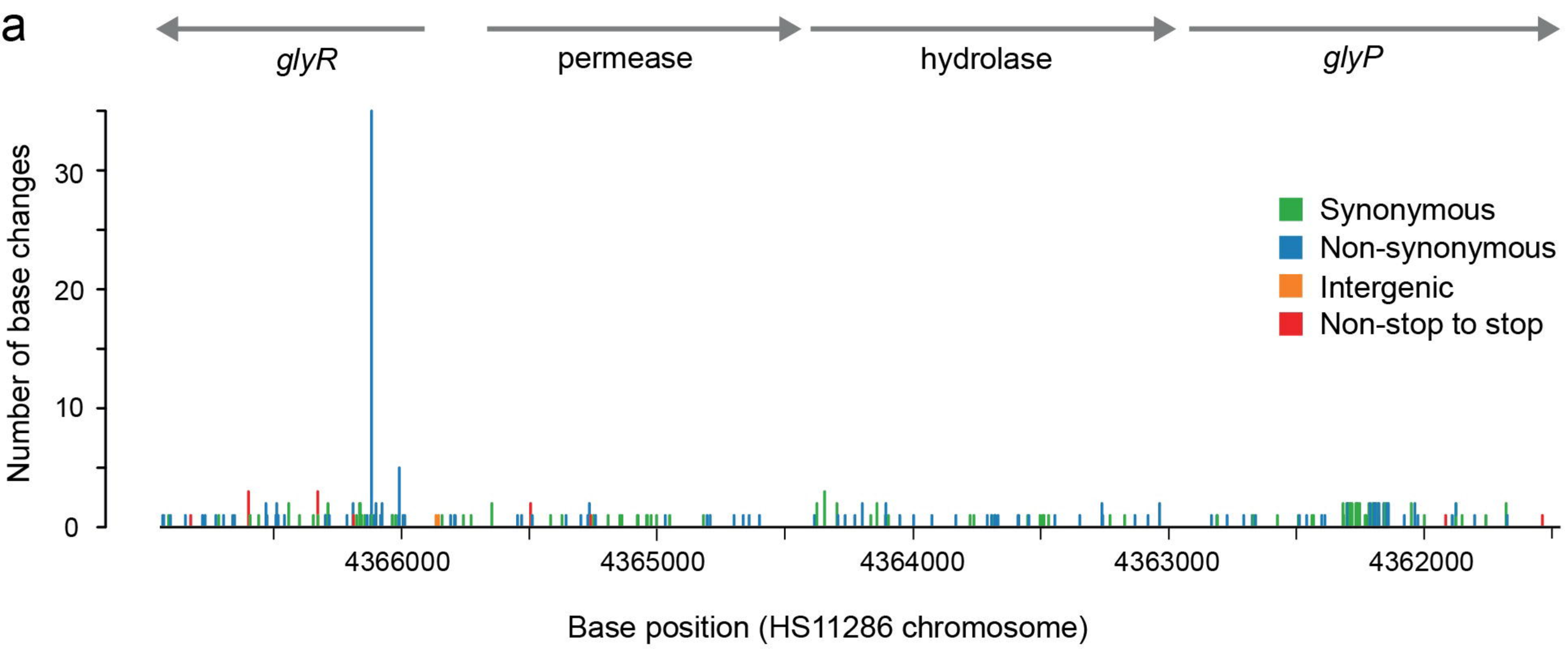
a
glyR
permease
hydrolase
glyP
Number of base changes
30
20
10
0
Synonymous
Non-synonymous
Intergenic
Non-stop to stop
4366000
4365000
4364000
4363000
4362000
Base position (HS11286 chromosome)

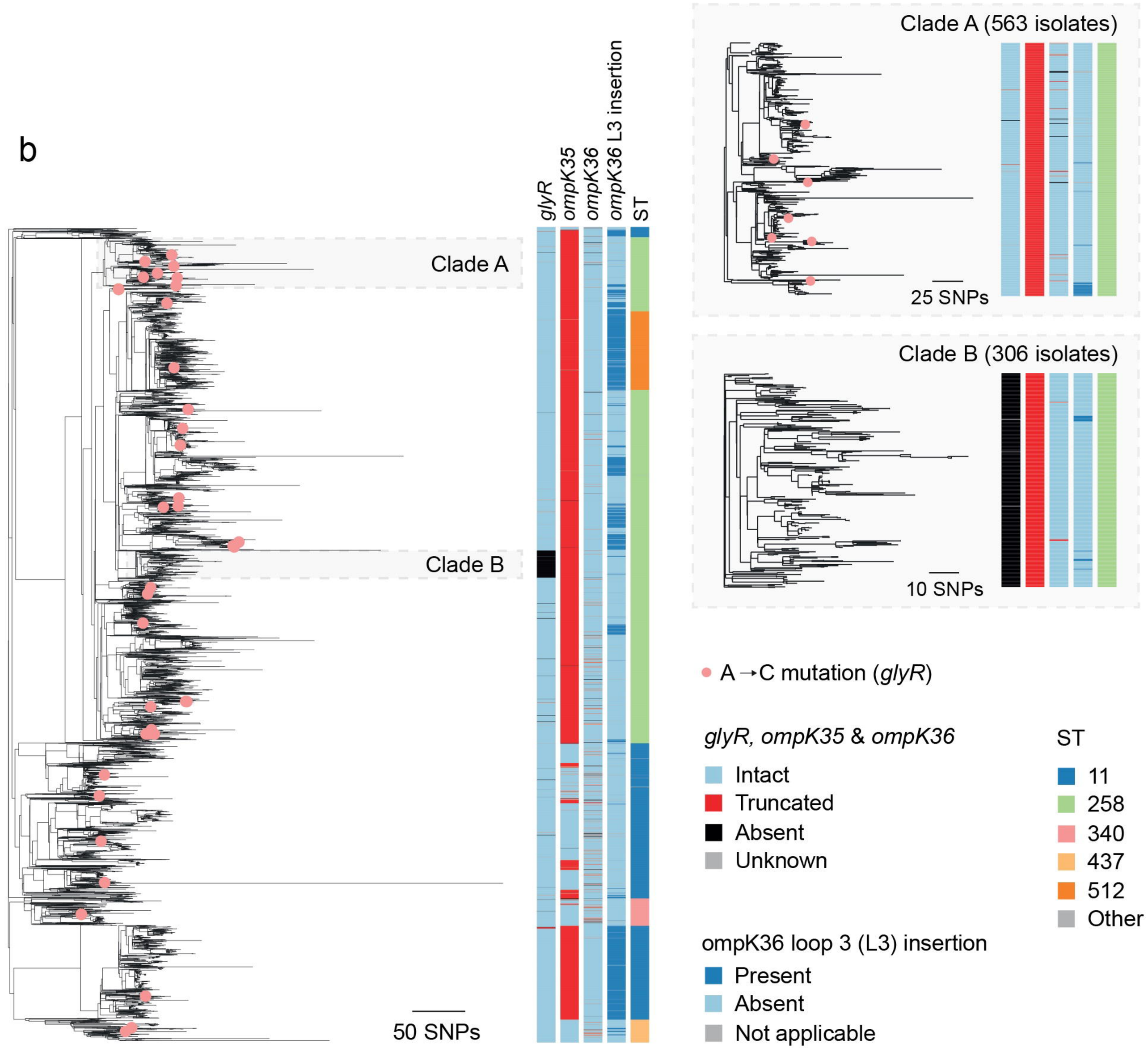
b
glyR
ompK35
ompK36
ompK36 L3 insertion
ST
Clade A
Clade B
50 SNPs
Clade A (563 isolates)
25 SNPs
Clade B (306 isolates)
10 SNPs
A→C mutation (glyR)
glyR, ompK35 & ompK36
Intact
Truncated
Absent
Unknown
ST
11
258
340
437
512
Other
ompK36 loop 3 (L3) insertion
Present
Absent
Not applicable